

Combustion completeness and sample location determine wildfire ash leachate chemistry

Micheline Campbell¹, Pauline C Treble², Liza Kathleen McDonough², Sebastian Naeher³, Andy Baker⁴, Pauline F Grierson⁵, Henri Wong², and Martin S Andersen⁴

¹UNSW Sydney

²ANSTO

³GNS Science

⁴University of New South Wales

⁵University of Western Australia

April 16, 2024

Abstract

Understanding past fire regimes and how they vary with climate, human activity, and vegetation patterns is fundamental to the mitigation and management of changing fire regimes as anthropogenic climate change progresses. Ash-derived trace elements and pyrogenic biomarkers from speleothems have recently been shown to record past fire activity in speleothems from both Australia and North America. This calls for an empirical study of ash geochemistry to aid the interpretation of speleothem palaeofire proxy records. Here we present analyses of leached ashes collected following fires in southwest and southeast Australia. We include a suite of inorganic elemental data from the water-soluble fraction of ash, as well as a selection of organic analytes (pyrogenic lipid biomarkers). We also present elemental data from leachates of soils collected from sites in southwest Australia. We demonstrate that the water-soluble fraction of ash differs from the water-soluble fraction of soils, with trace and minor element concentrations in ash leachates varying with combustion completeness (burn severity) and sample location. Changes in some lipid biomarker concentrations extracted from ashes may reflect burn severity. Our results contribute to building a process-based understanding of how speleothem geochemistry may record fire frequency and severity, and suggest that more research is needed to understand the transport pathways for the inclusion of pyrogenic biomarkers in speleothems. Our results also demonstrate that potential contaminant loads from ashes are much higher than from soils, with implications for the management of karst catchments, which are a critical water resource.

Hosted file

985278_0_supp_11799771_s7js1b.docx available at <https://authorea.com/users/721011/articles/705978-combustion-completeness-and-sample-location-determine-wildfire-ash-leachate-chemistry>

Combustion completeness and sample location determine wildfire ash leachate chemistry

Micheline Campbell¹, Pauline C. Treble^{2,1}, Liza K. McDonough², Sebastian Naeher³, Andy Baker^{1,2}, Pauline F. Grierson⁴, Henri Wong², and Martin S. Andersen⁵.

¹School of Biological, Earth, and Environmental Sciences, UNSW Sydney, Sydney, Australia.

²ANSTO, Lucas Heights, Australia

³GNS Science, Lower Hutt, New Zealand

⁴School of Biological Sciences, The University of Western Australia, Perth, Australia

⁵Water Research Laboratory, School of Civil and Environmental Engineering, UNSW Sydney, Sydney, Australia

Corresponding author: Micheline Campbell (micheline.campbell@unsw.edu.au)

Key points

- Stalagmites record past fire activity through changes in inorganic and organic chemistry, sourced from ashes.
- Wildfire ash leachate chemistry will aid interpretation of proxy fire data.
- Results show inorganic chemistry varies with burn severity and sample location, pyrogenic biomarker signal is less clear.

Abstract

Understanding past fire regimes and how they vary with climate, human activity, and vegetation patterns is fundamental to the mitigation and management of changing fire regimes as anthropogenic climate change progresses. Ash-derived trace elements and pyrogenic biomarkers from speleothems have recently been shown to record past fire activity in speleothems from both Australia and North America. This calls for an empirical study of ash geochemistry to aid the interpretation of speleothem palaeofire proxy records. Here we present analyses of leached ashes collected following fires in southwest and southeast Australia. We include a suite of inorganic elemental data from the water-soluble fraction of ash, as well as a selection of organic analytes (pyrogenic lipid biomarkers). We also present elemental data from leachates of soils collected from sites in southwest Australia. We demonstrate that the water-soluble fraction of ash differs from the water-soluble fraction of soils, with trace and minor element concentrations in ash leachates varying with combustion completeness (burn severity) and sample location. Changes in some lipid biomarker concentrations extracted from ashes may reflect burn severity. Our results contribute to building a process-based understanding of how speleothem geochemistry may record fire frequency and severity, and suggest that more research is needed to understand the transport pathways for the inclusion of pyrogenic biomarkers in speleothems. Our results also demonstrate that potential contaminant loads from ashes are much higher than from soils, with implications for the management of karst catchments, which are a critical water resource.

Plain Language Summary

Understanding past fire activity is necessary to develop effective land management strategies to both manage activity. Recently, stalagmites (naturally forming cave decorations) have been shown to record past fire information through chemical changes. The chemical

44 changes are due to post-fire leaching of wildfire ash. By investigating wildfire ash chemistry,
45 we will be able to improve our interpretations of the stalagmite past fire signal. Our results
46 show that ash chemistry from Australian fires varies with burn severity and sample location,
47 and that the ash chemistry and soil chemistry differ. Results suggest stalagmites may record
48 burn severity as well as fire frequency. We also suggest that the potential impact of high
49 concentrations of potential contaminants in wildfire ash on karst aquifers should be further
50 investigated.

51 **1 Introduction**

52 Wildfires occur on all ice-free continents, affecting about 40% of the terrestrial biome
53 (Chapin et al., 2011). Each year, an estimated ~300-460 million ha burn globally (Giglio et
54 al., 2006; Lizundia-Loiola et al., 2020; Wei et al., 2021). Globally, there has been an observed
55 increase in fire weather which has contributed to an increase in burned area in some regions
56 (noting that fire occurrence is modulated by more than just dangerous fire weather) (Jones et
57 al., 2022). Observational records are too short to fully understand fire regimes, so proxy
58 palaeofire data are sourced from natural archives such as sediment cores, ice cores, and tree
59 scars. These proxy archives have allowed past fire activity to be reconstructed at local (e.g.
60 Rehn et al., 2021), continental (e.g. Zennaro et al., 2015), and global scales (e.g. Marlon et
61 al., 2008).

62 Recent studies have shown that speleothems (cave formations such as stalagmites)
63 can record past fire activity via changes in both inorganic and organic chemistry. The
64 inorganic chemistry of karst dripwaters was shown to vary with cave depth, hydrogeology,
65 and fire severity (e.g. Treble et al. 2016; Nagra et al. 2016; Bian et al. 2019; Coleborn et al.
66 2018, 2019), with the strongest response in the most proxies observed in a shallow cave after
67 a severe fire (Bian et al. 2019). McDonough et al. (2022) demonstrated that an annually-
68 laminated stalagmite collected from a cave in Yanchep National Park, southwest Australia,
69 recorded all known fires to have burned over the cave through a suite of trace elements
70 (notably transition metals), colloidal organic matter content, growth rate, calcite $\delta^{18}\text{O}$, and
71 stalagmite fabrics. The annually laminated speleothem allowed for a coupled reconstruction
72 of past fire and climate, at very high resolution (annual resolution with a maximum age
73 uncertainty of ± 13 years over the 246-year long record) (McDonough et al., 2022). The
74 potential to reconstruct past fires at such high resolution and over long time periods
75 distinguishes speleothems from traditional palaeofire archives, which may be long, or high-
76 resolution, but rarely both (see Campbell et al. (2023)). Other research efforts have focused
77 on pyrogenic biomarkers, such as levoglucosan and polycyclic aromatic hydrocarbons
78 (PAHs) (Argiriadis et al., 2023, 2019; Homann et al., 2023, 2022), where elevated
79 concentrations of these pyrogenic biomarkers in speleothem calcite have been attributed to
80 past fire events. Generally, it is supposed that both inorganic and organic fire proxies are
81 sourced from ashes deposited over the cave, which are subsequently leached by rainfall, and
82 transported via karst flowpaths and deposited with speleothem calcite. Refining the
83 interpretation of speleothem palaeofire proxies calls for an empirical study of the
84 geochemistry of ash to inform the interpretation of both organic and inorganic speleothem
85 fire proxy records. While there are many studies of both laboratory and wildfire ash
86 chemistry, particularly within the context of contamination risk, this has not been done either
87 in karst environments or to understand ash chemistry within the context of speleothem
88 palaeofire records. Understanding wildfire ash chemistry in the karst environment also has
89 implications for water resources planning and contamination risk management.

90 Ash from combusted biomass is generally comprised of charred organic components
91 and minerals. At lower temperatures (usually $<450\text{ }^{\circ}\text{C}$) ash is mostly comprised of organic

92 carbon, while at higher temperatures (>450 °C), ash is comprised mostly of minerals as
93 inorganic carbonates, and at very high temperatures (>580 °C) most remaining minerals are
94 present as oxides (Certini, 2005; Bodí et al., 2014). Ash colour is generally related to
95 combustion completeness, with dark, organic-rich ashes formed at lower degrees of
96 combustion, and lighter mineral-rich ashes formed due to greater combustion completeness
97 (Bodí et al., 2014; Roy et al., 2010; Stronach and McNaughton, 1989). White ash is usually
98 more alkaline than black ash due to the solubilisation of major elements in ash (Bodí et al.,
99 2014; Pereira et al., 2012; Ulery et al., 1993), with ash pH generally ranging from 9.0 to 13.5
100 (Khanna et al., 1994; Misra et al., 1993; Yusiharni and Gilkes, 2012). Ash is an expected
101 source of certain elements owing to their sequestration within plant biomass, both living and
102 dead. Most biomass is comprised of C, with proportionally smaller amounts of H, O, N, P,
103 and S. Elements such as K, Na, Ca, Mg, Mn and Cl are taken up from the soil as ions for
104 functions including cellular structure and osmoregulation (Broadley et al., 2012; Kirkby,
105 2012). Fe, Mn, Cu and Zn are essential micronutrients but have low solubility, particularly in
106 alkaline calcareous soils, thus their uptake from soil solution requires them to be in a chelated
107 form. Calcium, Mg, K, Si, P, Na, S, Al, Fe, Mn, Zn, and associated carbonates (e.g., CaCO₃,
108 MgCO₃, and K₂CO₃) are normally the dominant inorganic constituents of ash (Bodí et al.,
109 2014; Gabet and Bookter, 2011; Pereira and Úbeda, 2010; Qian et al., 2009). However, their
110 relative amounts and proportions of different elements vary considerably as different
111 elements are volatilised to lesser or greater extent depending on the temperature of
112 combustion (Bodí et al., 2014; Hogue and Inglett, 2012). Concentrations of elements in ash
113 also reflects differences in sources, i.e., which tissues (leaf or wood) have been combusted, as
114 well as variation among species (e.g. Yusiharni and Gilkes, 2012). In a global analysis,
115 Sánchez-García et al. (2023) found that total extractable concentrations of the most abundant
116 constituents (organic C, Ca, Al, Fe, N, Mg, Na, and P, in order of mean abundance) were
117 variable, with large ranges. Mean concentrations ranged between 2.5 mg kg⁻¹ (P) to 204 g kg⁻¹
118 (organic C). Concentrations of the most abundant readily dissolvable constituents (organic
119 C, Ca, Na, Mg, PO₄, NH₄, Al, F, Mn, and Fe) were also variable, and mean concentrations
120 ranged between 1.3 mg kg⁻¹ (Fe) to 1103 mg kg⁻¹ (organic C). The ranges of the
121 concentrations they reported were generally consistent with other (local) studies reported in
122 the literature. Sánchez-García et al. (2023) reported that the variance in their ash
123 concentrations was due to the ecosystem, burn severity, land use history (resulting in. legacy
124 contamination) and leaching by rainfall prior to sample collection. Wildfires produce varying
125 ash amounts. Reported ash loads in Australia range between 6 Mg ha⁻¹ (Santín et al., 2015)
126 to 115.6 Mg ha⁻¹ (Santín et al., 2012), with ash load varying with burn severity and available
127 fuel load (Santín et al., 2015, 2012). In experimental settings, hotter combustion temperatures
128 have been shown to result in Ca/Mg ratios in ash leachates of <1 (Marion et al., 1991; Úbeda
129 et al., 2009). However, in ashes from both experimental studies and wildfires with known
130 burn temperature or severity (Balfour and Woods, 2013; Miotliński et al., 2023; Pereira et al.,
131 2012; Sánchez-García et al., 2023; Santín et al., 2015; Úbeda et al., 2009), the response of
132 both Ca and Mg to burn severity is variable, and none of the published concentrations support
133 the hypothesis that this ratio indicates burn severity.

134 In speleothems, trace elements are derived from soil as well as soluble ash products.
135 Fires affect soils in many ways, including alterations to soil organic matter (SOM), decreased
136 cohesion, increased soil water repellence, and altered soil chemistry (Campos et al., 2015;
137 Certini, 2005; DeBano, 2000; Pellegrini et al., 2022; Roshan and Biswas, 2023). Ash
138 deposition has been shown to both directly and indirectly alter soil chemistry. Soil pH,
139 exchangeable ions (Na⁺, K⁺, Ca⁺, and Mg⁺), total N, and available PO₄, are consistently
140 higher post-fire, particularly in association with ash beds (Adams and Boyle, 1980; Certini,
141 2005; Humphreys and Lambert, 1965; Khanna et al., 1994; Serrasolsas and Khanna, 1995).

142 These effects can persist for months (e.g. Granged et al. (2011)) to years after fire (e.g.
143 Muñoz-Rojas et al., 2016). Fire impact on soils is largely determined by fire intensity and
144 duration, which is a function of the ecosystem and climate (Roshan and Biswas, 2023;
145 Shakesby and Doerr, 2006), Surface soils also tend to be more affected than deeper soils
146 (Bento-Gonçalves et al., 2012; Bradstock and Auld, 1995; Williams et al., 2004). Soil
147 moisture further modulates both fire temperature at the soil surface and temperature
148 penetration. In moist soils, temperatures tend to be lower until soil moisture is vapourised,
149 however, moist soils tend to transport heat more quickly and therefore deeper (Campbell et
150 al., 1994; Certini, 2005). Consequently, the impact of fires on soils, and the recovery of those
151 soils to pre-fire conditions, is difficult to predict, and soil impacts and recovery are likely to
152 vary in both time and space.

153 The legacies of fire impacts on ash and soil are also evident in organic compounds
154 resulting from the combustion of plant material. Pyrogenic biomarkers such as levoglucosan
155 and polycyclic aromatic hydrocarbons (PAHs) are used to investigate past fire activity in
156 environmental archives such as ice and sediment cores, and speleothems (Argiriadis et al.,
157 2019, 2023; Denis et al., 2012; Homann et al., 2022, 2023; Rubino et al., 2016; Vachula et al.,
158 2019). Levoglucosan (1,6-anhydro- β -d-glucopyranose) is a water-soluble anhydrosugar
159 which is formed through the thermal breakdown of cellulose and hemicellulose (Bhattarai et
160 al., 2019; Elias et al., 2001; Li et al., 2021; Simoneit et al., 1999). Levoglucosan is source
161 specific, and unlike other pyrogenic biomarkers, is not produced by the combustion of fossil
162 fuels, making it a reliable tracer of biomass burning (Elias et al., 2001). While normally
163 associated with particulate matter and smoke, levoglucosan has been shown to be present in
164 black char (Kuo et al., 2008; Otto et al., 2006). Levoglucosan yield from black char has been
165 shown to vary with temperature and plant species (Kuo et al., 2008). Levoglucosan is semi-
166 volatile and can be transported with smoke in the atmosphere, where it has an atmospheric
167 life of \sim 26 days (Bai et al., 2013). PAHs are organic molecules characterised by two or more
168 aromatic rings which form by incomplete combustion of biomass and fossil fuels. In the
169 modern era anthropogenic inputs (e.g. fossil fuels) are the dominant source, and in sediment
170 cores the most recent deposits can be greatly enriched relative to pre-industrial levels
171 (Perrette et al., 2008; Wakeham et al., 1980). The amount and type of PAHs formed by fire is
172 controlled by the maximum temperature, duration, and oxygen level (Blumenstock et al.,
173 2000; Johansson and van Bavel, 2003). At temperatures up to 400 °C, low molecular weight
174 PAHs (<252 g/mol; 4-ring compounds) are more abundant in post-fire soils than high
175 molecular weight PAHs (>252 g/mol; 5-ring compounds) (Kim et al., 2011; Rey-Salgueiro et
176 al., 2018; Simon et al., 2016). Karp et al. (2020) describe a temperature optimum for PAH
177 formation between 400 °C and 600 °C. Low PAH yield at low temperature is explained by
178 incomplete condensation of \leq 2 ring PAHs, while low yield at high temperature is explained
179 by either complete combustion of the PAHs, or their incorporation into larger particles (>8
180 rings) (Karp et al., 2020). While PAHs adsorb onto organic matter, which limits degradation
181 and bioavailability, levels in post-fire soils have been shown to decline to pre-fire
182 concentrations over time as leaching and erosion mobilises PAHs (Kim et al., 2011; Simon et
183 al., 2016; Yang et al., 2010). Degradation of PAHs has also been shown to occur in soil
184 samples stored at ambient temperatures (Douglas et al., 2018; Rost et al., 2002). However,
185 Douglas et al. (2018) showed that the PAHs chrysene and pyrene were resistant to
186 degradation under ambient temperatures over the 30 day study. Some research has attributed
187 high soil PAH levels to ash deposition, while others have suggested that the ash bed is not a
188 source of PAHs for soils, and that PAHs are instead mobilised and transported to waterways
189 rather than infiltrating (Kim et al., 2011; Simon et al., 2016). In speleothems, it is unclear
190 whether the pyrogenic biomarker signal is transported via the leaching of deposited ashes
191 over the cave, or via aerosol inputs (Homann et al., 2023), although Homann et al. (2022)

192 sampled cave dripwaters and demonstrated that in that cave levoglucosan was transported via
193 the epikarst. Analyses of pyrogenic biomarkers in wildfire ash will contribute to building a
194 process-based understanding of pyrogenic biomarkers as speleothem proxies.

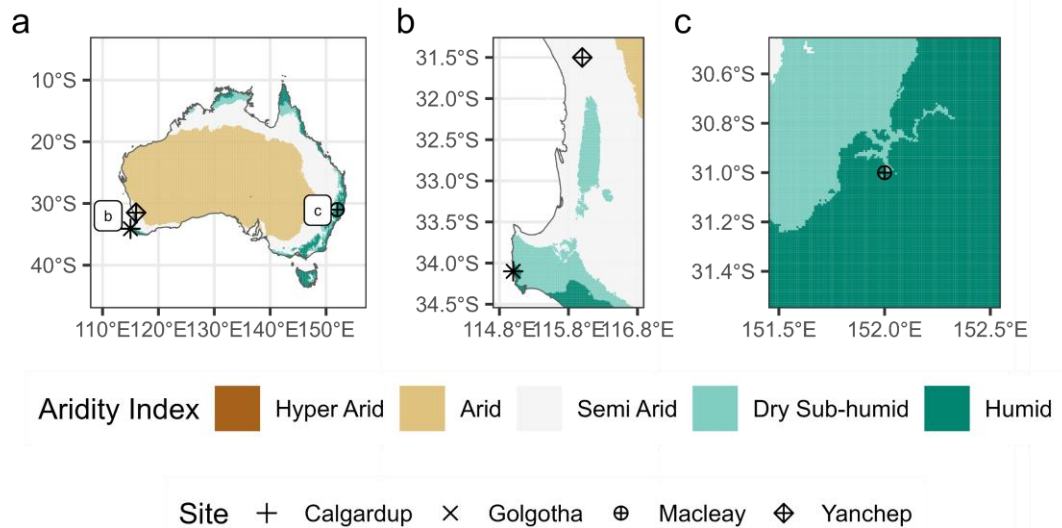
195 Speleothems are excellent geochemical archives of past surface environmental change
196 (e.g., Cheng et al., 2016; Domínguez-Villar et al., 2009). While speleothem proxies have
197 recently been used to investigate past fire (see Argiriadis et al., 2023; Homann et al., 2023,
198 2022; McDonough et al., 2022), a process-based understanding of the formation of fire
199 proxies (both organic and inorganic) and how they reflect fire activity is needed to 1) build
200 confidence in speleothems as archives of past fire, and 2) determine whether and how
201 speleothems can record past fire severity as well as frequency. Here we present analyses of
202 inorganic proxies in the water-soluble fraction of ash and soil samples collected from
203 southwest and southeast Australia, and organic pyrogenic biomarkers from the solvent-
204 extracted fraction of ashes. We present a suite of elemental data, as well as electrical
205 conductivity, pH, and alkalinity, for ash and soil leachates, as well as a limited number of
206 pyrogenic biomarkers for a subset of ash samples. Results presented here will aid the
207 interpretation of both organic and inorganic palaeofire proxy data in natural archives such as
208 speleothems and sediment cores.

209 **2 Site description and methods**

210 **2.1 Site descriptions**

211 **2.1.1 Southwest Australia**

212 We collected ash and soil samples from two regions in southwest Australia: the
213 Yanchep National Park in the Perth region and Leeuwin-Naturaliste National Park in the
214 Capes region (Figure 1). Yanchep National Park is located ~47 km north of Perth, Western
215 Australia. The underlying geology is the Tamala Limestone, a Pleistocene aeolianite
216 (Playford et al., 1976). The climate is characteristically Mediterranean, with cool, wet winters
217 and hot, dry summers, with most rainfall occurring during the winter (McDonough et al.,
218 2022). Vegetation in the generally region follows a progression inland from dune vegetation
219 dominated by sedges, rushes, and rhizomatous grasses, to coastal heath, limestone heath, and
220 then *Banksia*-dominated woodland, with some wetland present (Fontaine, 2022). Eucalypt
221 and *Melaleuca* woodlands are also widespread. Ash samples were collected at Yanchep in
222 January 2020, following a severe wildfire in December 2019 from a region of the National
223 Park where vegetation is comprised of a tuart (*Eucalyptus gomphocephalla*) overstorey with
224 and understorey of *banksia* heath, interspersed by occasional wetland. The 2019 fire burned
225 ~12300 ha, but with some variability, such that a range of severity classes are represented
226 (Fontaine, 2022). An analysis of the differenced Normalised Burn Ratio (dNBR; see Text S1)
227 shows that the most common severity class was ‘Moderate-high severity’, representing ~5200
228 ha (dNBR between 0.44 and 0.659; Key and Benson, 2006). See Text S1 for a dNBR map of
229 this event. Soil samples were collected from two sites within Yanchep National Park in 2022,
230 see Section 2.3 for the sampling protocol.



231

232 **Figure 1 Map of Australia showing the four ash collection locations. Aridity Index is**
 233 **also mapped, according to Zomer et al., (2022). a) Australia, with collection sites**
 234 **indicated. b) southwest WA, with collection sites at Yanchep, Calgardup Caves, and**
 235 **Golgotha Cave indicated. c) the Macleay region, with collection site indicated. The base**
 236 **Australia map is the GEODATA TOPO 250K Series 3 (Geoscience Australia, 2006).**

237 Both ash and soil samples were collected from above the Calgardup and Golgotha
 238 caves in the Capes region of southwestern Western Australia, between Cape Leeuwin and
 239 Cape Naturaliste (Figure 1). As for Yanchep, the underlying geology is Tamala Limestone,
 240 and the climate is also Mediterranean, although annual precipitation is higher and
 241 temperatures are more moderate than Yanchep. The vegetation community at Golgotha Cave
 242 is eucalypt open forest characterized by a mixed canopy of marri (*E. calophylla*) and jarrah
 243 (*E. marginata*) with occasional karri (*E. diversicolor*) on the ridge above the cave, and tall
 244 open karri forest below the cave. The understorey is a mix of *Agonis flexuosa*, *Trymalium*
 245 *spathulatum*, *Podocarpus drouynianus*, *Xanthorrhoea preissi*, *Bossiaea disticha* and
 246 *Templetonia retusa* (Treble et al., 2016). The Golgotha Cave ash samples were collected in
 247 January 2022, following a wildfire in December 2021 which burned nearly 8000 ha in the
 248 Leeuwin-Naturaliste National Park (DBCA-060 Fire History database;
 249 <https://catalogue.data.wa.gov.au/dataset/dbca-fire-history>). Of those ~8000 ha, ~5400 ha are
 250 classified by dNBR as being of ‘High Severity’ (dNBR > 0.66; Key and Benson, 2006), and
 251 ~1400 ha classified as ‘Moderate-high severity’ (dNBR between 0.44 and 0.659; Key and
 252 Benson, 2006). See Text S1 for a dNBR map of this event.

253 Dominant vegetation at Calgardup Cave is low open forest of jarrah and marri with a
 254 dense and diverse understorey comprised mainly of *Banksia*, *Xanthorrhoea*, *Hakea*, and
 255 *Melaleuca* species close to the cave entrance, but which grades into a mix of marri-jarrah and
 256 karri to the southwest. The Calgardup Cave ash samples were collected in August 2018 one
 257 day after a low-intensity prescribed burn. The fire was small, highly localised, and cloud
 258 cover too heavy for dNBR analysis of this event. However, post fire condition showed that no
 259 canopy was burnt and that severity was overall low. Soil samples were collected
 260 opportunistically from above both the Calgardup and Golgotha caves, and from six other sites
 261 in the Leeuwin-Naturaliste National Park between 2006 and 2022.

262 2.1.2 Southeast Australia

263 Ashes were collected from the Macleay Karst Arc, located in the Mid North Coast of
264 New South Wales (NSW), southeast Australia (Figure 1). The underlying geology is a
265 Permian limestone, comprised of a basal calcareous mudstone, a central unit of crinoidal
266 limestone, and discontinuous reef limestones (NSW Department of Environment, Climate
267 Change and Water, 2011). The climate is temperate humid sub-tropical, with strong
268 temperature seasonality, and a seasonal bias in precipitation with most precipitation occurring
269 in summer (Baker et al., 2020). Vegetation is varied, with some subtropical rainforest,
270 interspersed with cleared areas. Ash samples were collected in February 2020 following the
271 Carrai East fire, which burned from October 2019 to January 2020 during the Australian
272 ‘Black Summer’ fire season. The fire burned ~150278 ha (NSW Rural Fire Service, 2020).
273 dNBR analyses suggest that this includes ~42000 ha burned at high severity, and ~75000 ha
274 at moderate-high severity, noting that the unusual length of the event (two months) may have
275 skewed dNBR results (see Text S1).

276 No soil samples were collected from southeast Australia, as the site was not accessible
277 due to extensive flood damage in 2022 following the fires in 2019/2020.

278 2.2 Fire histories

279 Fire histories for each site were extracted from databases. The Western Australian
280 Department of Biodiversity, Conservation, and Attractions (DBCA) maintains a spatial
281 dataset of known fires in Western Australia (DBCA-060 Fire History), with fire event
282 polygons, fire type, fire size, and approximate dates, among other fields
283 (<https://catalogue.data.wa.gov.au/dataset/dbca-fire-history>, accessed November 2022). The
284 earliest fires recorded in the database are from 1937, and known issues include missing
285 events and inaccurate dating (Dixon et al., 2022). The New South Wales National Parks and
286 Wildlife Service (NPWS) maintains a dataset of wildfire and prescribed burn events which
287 occurred within the NPWS estate, as well as some fire events which occur or extend beyond
288 the estate (NPWS Fire History – Wildfires and Prescribed Burns;
289 <https://datasets.seed.nsw.gov.au/dataset/fire-history-wildfires-and-prescribed-burns-1e8b6>,
290 accessed in November 2022). The database includes fields which describe the fire extent and
291 type of fires which have occurred since 1920, and was last revised in October 2022.

292 The two fire history databases were interrogated using *QGIS (3.28.0)* and *R (version*
293 *4.3.1)*, with the *dplyr (1.1.2)*, *sf (1.0.14)*, and *rgdal (1.6.7)* packages (Bivand et al., 2021;
294 Pebesma, 2018; QGIS Development Team, 2022; R Core Team, 2023; Wickham et al.,
295 2020)), and fire histories for each ash and soil sampling location were extracted. Scripts
296 detailing this process are available in the supplementary dataset (Campbell et al., 2024).
297 These fire histories are represented in the dataset as two variables – the number of years since
298 the last fire prior to collection (i.e. the penultimate fire for ash samples), and the total number
299 of fires experienced for each sample location. Some manual corrections were made to the fire
300 histories where the spatial resolution of the database was sufficient to accurately delineate
301 between burned and unburned sites at the fire edge. Where the location had not experienced a
302 fire during the observational period (i.e. 8 of the 9 Macleay samples), the years since last fire
303 was given as 100 years, the length of the NPWS database.

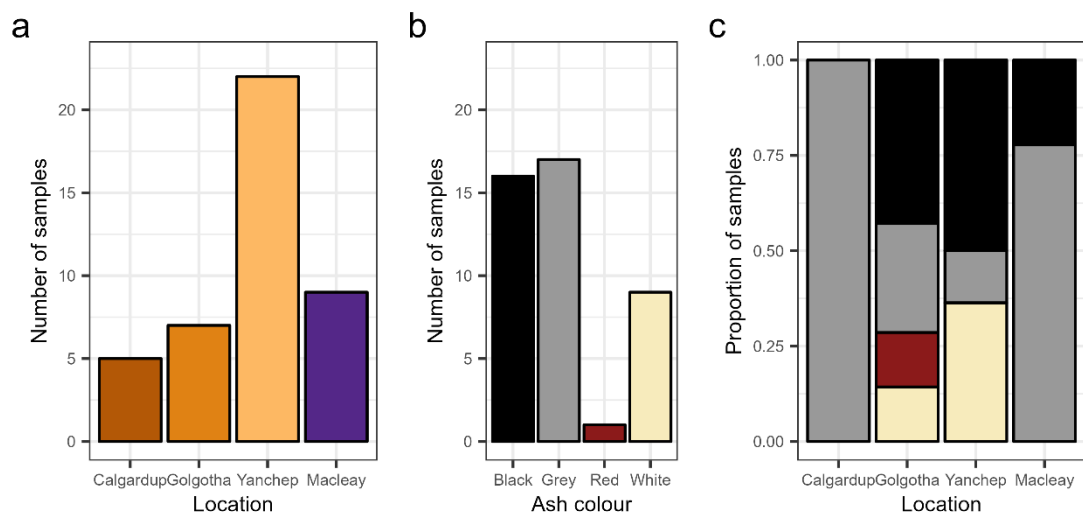
304 For the length of the fire history databases, most sample sites had experienced at least
305 one fire during the observational period, with a median number of fires of four and a
306 maximum of nine. Of the sampling sites, Macleay sites had had the fewest total fires,
307 Yanchep sites had experienced between three and nine fires, Golgotha Cave experienced
308 between four and five fires, and Calgardup Cave had five recorded fires.

309 The median period since the last fire for all sample locations was 14 years, and 88%
 310 of sample locations had burned in the 50 years prior to collection. For the ash samples,
 311 sample sites above Calgardup Cave and at Yanchep had burned most recently (years since
 312 previous fire were 10 and 14 years, respectively). Sample locations above Golgotha Cave
 313 sample locations were last burned 16 years before sample collection. Most Macleay sample
 314 locations had no recorded fires, but one sample location had burned 18 years prior to sample
 315 collection.

316 2.3 Sampling protocols

317 Forty-three ash samples were opportunistically collected following fire events at the
 318 sites described above. Ash samples were collected one day after fire at Calgardup Cave, ~1
 319 month post-fire at Golgotha Cave and Yanchep National Park, and within maximum three
 320 months of the fire at Macleay. Ashes were classified according to a simple colour
 321 classification: black, grey, red, and white (Figure 2). Ash sampling was targeted for inorganic
 322 analyses in the first instance. Plastic equipment was used to collect and store the samples to
 323 avoid contamination with metals. At Golgotha Cave (the most recent site sampled), a
 324 duplicate dataset was collected specifically for organic geochemistry analyses. These samples
 325 were collected using metal implements and stored in aluminium foil to minimise plastic
 326 contamination. A limited number of samples from Yanchep, Calgardup Cave, and Macleay
 327 which were collected with the inorganic sampling protocol were subsequently also analysed
 328 for lipid biomarkers. Samples collected for inorganic analyses were stored in plastic zip loc
 329 bags in a cool storage room. Samples collected for organic analyses were stored in aluminium
 330 foil in a cool storage room.

331 Ash samples are not evenly distributed by either site or ash colour. A greater number
 332 of samples were collected at Yanchep, with the fewest samples collected at Calgardup Cave
 333 (Figure 2). More grey and black samples ($n = 17$ and $n = 16$, respectively) were collected
 334 than red and white samples ($n = 1$ and $n = 9$; Figure 2). This is due to the opportunistic
 335 nature of sampling, which largely relied on volunteer efforts.



336
 337 **Figure 2** The distribution of ash samples by location (a), ash colour (b), and both
 338 location and ash colour (c).

339 A total of 44 soil samples were collected from ten sites in southwest Australia in 2006,
340 2015, and 2022. The 2006 and 2015 sampling targeted the Capes region sites, while 2022
341 sampling targeted both the Capes region and Yanchep National Park (see Table S1 for a list of
342 soil sampling locations). The 2006 samples collected from Golgotha Cave were collected as
343 part of sample collection for Treble et al. (2016), while 2015 Capes region samples were
344 targeted at sites that had experienced recent fire (e.g. Moondyne in 2003) and sites which had
345 not burned in decades (e.g. Jewel Cave which last burned in 1961). 2022 sampling was
346 undertaken on sites which had burned in recent years at both Yanchep and in the Capes
347 region, some of which had previously been sampled in 2006 and/or 2015. Sampling protocol
348 was to collect soil at depths of 0-10 cm, and 10-20 cm (for one sample only the top 5 cm of
349 soil was collected). For statistical analyses, all samples are categorised as sampled from 0-10
350 cm or 10-20 cm. Samples were not evenly selected by site or location, with a larger number
351 of samples collected from the Capes region than from Yanchep. More than 20% of samples
352 were collected at Golgotha Cave.

353 **2.4 Inorganic analyses**

354 Inorganic geochemistry was undertaken on all ash and soil samples at the Isotope
355 Tracing in Natural Systems laboratory at ANSTO, Lucas Heights, Australia. Ash leachates
356 were extracted from unhomogenised samples using the USGS field leach test (Hageman,
357 2007). Sample was mixed with deionised water at a ratio of 1:20 by weight, agitated for 15
358 minutes, and then rested for 10 minutes. The supernatant was filtered using 0.45 μm pore-size
359 nitrocellulose filters and alkalinity and pH measurements were performed using a Metrohm
360 862 Compact Titrosampler following Standard Methods for the Examination of Water and
361 Wastewater, Method 4500-CO₂ D. Carbon Dioxide and Forms of Alkalinity by Calculation
362 (American Public Health Association, American Water Works Association, Water
363 Environment Federation et al., 2017). Electrical conductivity (EC) for a subset of samples
364 was measured by Radiometer CDM92 conductivity meter. A sub-sample was acidified with
365 Merck Suprapur HNO₃ to 1% (vol/vol) for cation analysis by inductively coupled plasma
366 atomic emission spectroscopy (ICP-AES) and inductively coupled plasma mass spectrometry
367 (ICP-MS), and an unacidified portion retained for anion measurement by ion chromatography
368 (IC). Samples were stored in laboratory refrigeration at 4 °C prior to analysis. To analyse a
369 majority of (including volatile) elements, soil leachates were prepared as received to maintain
370 their integrity. One batch of samples (2022/0199) were subsequently corrected for moisture
371 content for report consistency with the other samples, as they were moist when collected –
372 see Text S2 for correction equations.

373 The charge balance error (%) was calculated for ash and soil leachates in PHREEQC.
374 For ash leachates, total alkalinity, pH, Ca, K, Mg, Na, Si, P, Sr, Ba, Br, F, Cl, SO₄ and NO₃
375 were used as the input variables, with a temperature of 25 °C. Forty-three of the 58 samples
376 (including replicates) returned charge balance errors within $\pm 10\%$, while 23 samples returned
377 charge balance errors within $\pm 5\%$ (noting that the charge balance was calculated on replicates
378 separately; see Table S2 and Figure S1 for charge balance errors). The largest proportion of
379 leachates with a positive charge imbalance were from black ashes (~47% of black ash
380 samples $> +10\%$ error), while only one grey ash leachate sample, and no white or red
381 samples had a charge balance error $> +10\%$. The positive charge imbalance for the black ash
382 samples may be attributed to the higher proportion of organic matter typically found in black
383 ashes (Bodí et al., 2014), which may have resulted in higher dissolved organic carbon
384 concentrations in the leachates. This can result in organic anions contributing significantly to
385 the charge balance. This is not accounted for in the PHREEQC charge balance calculation,
386 which includes only inorganic ions (Dasgupta et al., 2015). Three ash leachates returned
387 charge balance errors $< -10\%$, two of which were $< -40\%$. All three negatively charged

388 leachates were samples from the Macleay region. Most Macleay samples had charge balance
389 errors < -5% (see Table S2).

390 Charge balance error was calculated for only 27 of 63 soil leachates (including
391 replicates), due to missing pH data. For soil leachates, the input variables were total
392 alkalinity, pH, Ca, Fe, K, Mg, Na, P, Br, Ba, Sr, Cl, SO₄, and NO₃, with a temperature of 25
393 °C. Twenty-two of the 27 samples returned a charge balance error within ±10%, and 11/27
394 returned a charge balance error within ±5% (see Table S3). One sample, collected at
395 Yonderup, returned a charge balance error of ~+39%. Due to the small sample size, and
396 uncertainty around the charge balance of the samples which could not be calculated using
397 PHREEQC, no data were excluded from the subsequent statistical analyses.

398 Preliminary analysis of a subset of the ash data (nine variables measured in 16
399 samples from Yanchep National Park) was previously presented as a case study in Campbell
400 et al. (2023). Results presented there showed that the ash leachate chemistry differed between
401 black and white ashes (n = 16). This supported the hypothesis of McDonough et al. (2022)
402 that speleothem palaeofire trace element proxies are sourced from ash.

403 2.5 Biomarker analyses

404 Biomass burning biomarkers (levoglucosan and PAHs) were analysed in the
405 GNS/VUW Organic Geochemistry Laboratory at GNS Science, New Zealand. Freeze-dried,
406 homogenised ash (0.33–0.95 g) samples were extracted three times with dichloromethane/
407 methanol (3:1, v:v) by ultrasonication for 20 min each time, followed by centrifugation at
408 2000 rpm for 5 min. The resulting extracts were filtered on cotton wool-plugged Pasteur
409 pipettes and evaporated under N₂ at 35 °C to obtain dried total lipid extracts (TLEs). Half of
410 each TLE was derivatized with 50 µL *N,O*-bis(trimethylsilyl)trifluoroacetamide (BSTFA)
411 with 1% trimethylchlorosilane (TMCS) at 70 °C for 1h. After cooling, the solutions were
412 evaporated under N₂ at 35 °C until dryness and redissolved in *n*-hexane for analysis.

413 The derivatised TLEs were analysed by gas chromatography mass spectrometry (GC-
414 MS) on an Agilent 7890A GC System, equipped with an Agilent J&W DB-5ms capillary
415 column [60 m × 0.25 mm inner diameter (i.d.) × 0.25 µm film thickness (f.t.)], and coupled
416 through a split to an Agilent 5975C inert MSD mass spectrometer and a flame ionisation
417 detector (FID). The temperature programme of the oven was 70 °C to 130 °C at 20 °C min⁻¹,
418 then at 4 °C min⁻¹ to 320 °C and held isothermal for 15 minutes, which results in a total run
419 time of 65.5 min. Helium was used as carrier gas with a constant flow of 1.0 mL min⁻¹.
420 Samples (3 µL) were injected splitless at an inlet temperature of 300 °C. The MS was
421 operated in electron impact ionisation mode at 70 eV using a source temperature of 230 °C.
422 After a solvent delay of 10 min, samples were analysed in full scan mode with *m/z* 50–700.

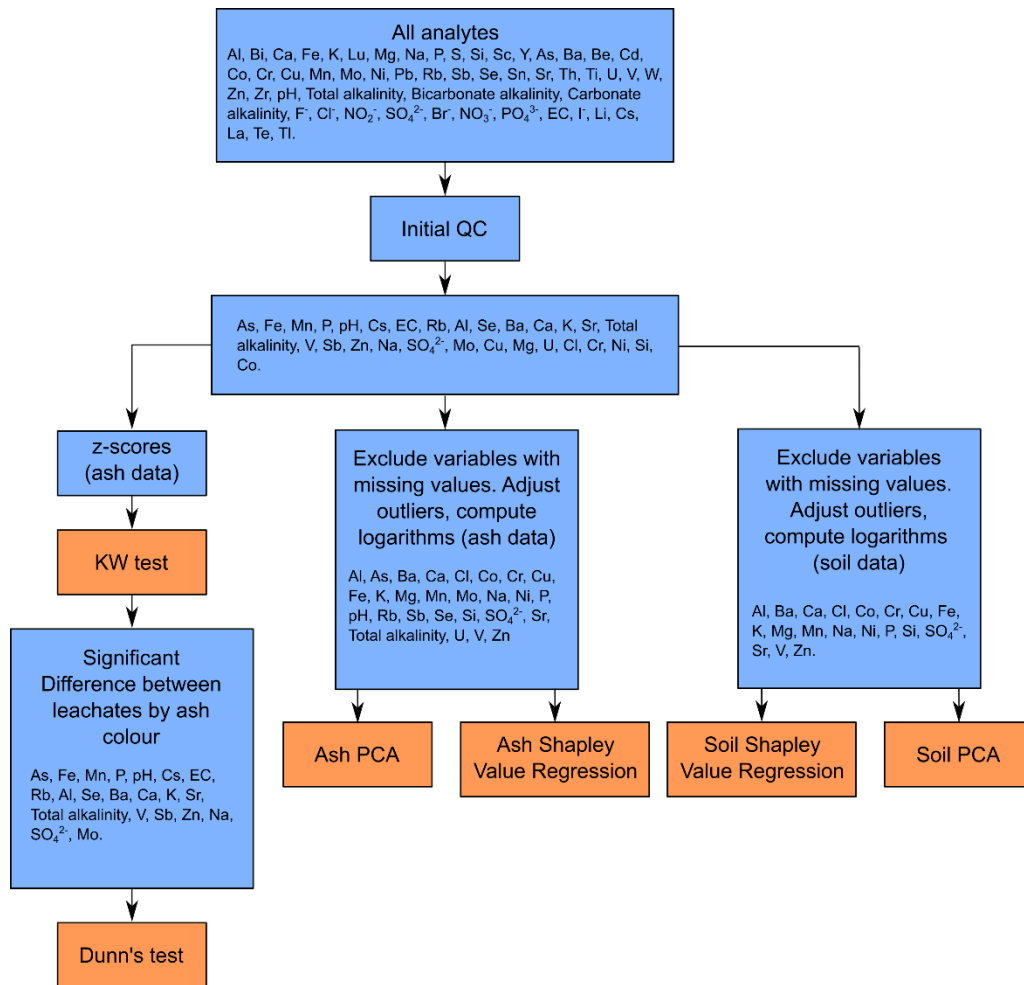
423 Internal standards (5 α -cholestane, *n*-nonadecanol and *n*-nonadecanoic acid) for
424 quantification were added to the samples prior to the first extraction. Procedural blanks and
425 laboratory reference standards were also analysed to ensure data quality and absence of
426 laboratory contaminants.

427 Analyses of Golgotha Cave ash samples were repeated in November 2023 to test for
428 alteration of the biomarker signal *ex situ*. The same sample protocol as above was followed,
429 except larger sample sizes (up to 2.81 g) were used.

430 2.6 Software and statistical methods

431 Data were analysed and visualized using the statistical software *R* (version 4.3.1), and
432 the packages *readr* (2.1.4), *dplyr* (1.1.2), *ggplot2* (3.4.2), *boot* (1.3-28.1), *ShapleyValue*
433 (0.2.0), *stringr* (1.5.0), *tidyr* (1.3.0), *ggbiplot* (0.55), *EnvStats* (2.8.0), *purr* (1.0.1), and *stats*
434 (4.3.1) (Canty and Ripley, 2022; Davison and Hinkley, 1997; Liang, 2021; Millard, 2013; R

435 Core Team, 2023; Vu, 2011; Wickham, 2022, 2016; Wickham et al., 2023, 2020; Wickham
 436 and Henry, 2023). Fire history databases were clipped to the study sites in QGIS (3.28.0)
 437 before interrogation in R (QGIS Development Team, 2022). Figure 3 shows the data
 438 processing workflow and the analytes used for each statistical test.



439
 440 **Figure 3 the workflow for the data processing and statistical analyses of inorganic**
 441 **leachate data. Orange boxes indicate a statistical test, blue boxes indicate a data**
 442 **processing step.**

443 Where replicate leachates were analysed, the results were combined and the means
 444 used in the statistical analyses. Outliers in the soil and ash leachates chemistry were identified
 445 using Rosner's Test in the R package 'EnvStats', which allows for multiple outliers to be
 446 identified (Millard, 2013; Rosner, 1983). Outlier identification was adapted from a script
 447 presented in Croke et al. (2021). As the sample sizes for soil (n = 43) and ash (n = 44)
 448 leachates are small, outliers were replaced with the median value rather than removed.
 449 Histograms of the data distributions for both soil and ash leachates with outliers indicated are
 450 found in Figures S2 and S3. Histograms show that geochemistry data are all skewed,
 451 necessitating either transformation or non-parametric statistical tests. Initial quality control
 452 was conducted to limit the number of analytes included in the statistical analyses (see Text S3
 453 for details).

454 To test how ash chemistry changes with ash colour, we applied the non-parametric
 455 Kruskal-Wallis rank sum test to determine if there was significant difference in ash chemistry
 456 between ash colours (Hollander and Wolfe, 1973). To minimise the impact of location on ash
 457 chemistry, data were first grouped by location and then transformed to z-scores. The null

458 hypothesis of the Kruskal-Wallis test is that samples originate from the same distribution,
459 with the alternative hypothesis that the samples originate from different distributions. A
460 significant Kruskal-Wallis result indicates that there is some difference in the distributions,
461 but it cannot tell where that difference occurs. Dunn's Test is the nonparametric post-hoc test
462 for multiple comparisons (Dunn, 1964), and shows which variables are significantly different
463 from one another. The null hypothesis is that there is no difference between groups, while the
464 alternative hypothesis is that there is a difference between groups. Importantly, Dunn's test
465 allows for groups to be of equal or unequal size.

466 Shapley Value regression allows for the relative importance of predictor variables in
467 linear regression to be calculated. It achieves this by computing the R-squared for each
468 possible combination of predictor variables and calculating the average improvement when
469 adding a variable to a model (Budescu, 1993; Lipovetsky and Conklin, 2001). Shapley value
470 regression was undertaken on the ash and soil leachate data using the *ShapleyValue* package
471 in *R* (Liang, 2021; R Core Team, 2023). For the ash samples, the predictors were ash colour,
472 location, years since the last fire, and the total number of fires. For the soil sample analyses,
473 the predictors were sample depth, location, years since the last fire, and the total number of
474 fires. For both ash and soil data, values were log-transformed (base 10) prior to analyses.
475 Confidence Intervals (CIs) were calculated at $\alpha = 0.95$ using the bias corrected and
476 accelerated intervals (BCa) on bootstrap replicates of the standardised Shapley values ($R =$
477 5000). Bootstrap resampling and calculation of CIs were done using the *boot* package in *R*
478 (Canty and Ripley, 2022; R Core Team, 2023). BCa intervals were used to calculate CIs as it
479 is the only method which is guaranteed to return intervals within the statistics sampling space
480 (0-1), and is in general recommended, given sufficient sample n and bootstrap replicates
481 (Carpenter and Bithell, 2000; Puth et al., 2015)

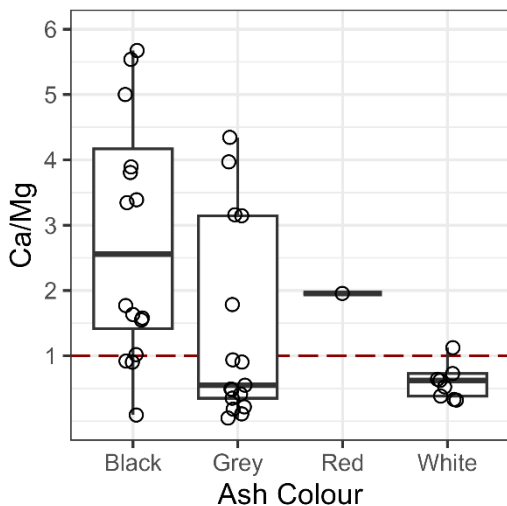
482 Principal component analyses (PCA) were performed using the '*prcomp*' function in
483 *R* on the logarithm (base 10) of the inorganic leachate data (R Core Team, 2023). The PCAs
484 were done on the correlation matrix, and data were mean subtracted. Where zeroes were
485 introduced due to how values less than the limit of detection were handled (by replacing
486 those values with a random number between zero and the limit), these zeroes were replaced
487 with the minimum measured value for that variable. Figures S2 and S3 show the distributions
488 of the input data.

489 **3 Results**

490 **3.1 Ash**

491 **3.1.1 Relationships between ash colour, chemistry and burn severity**

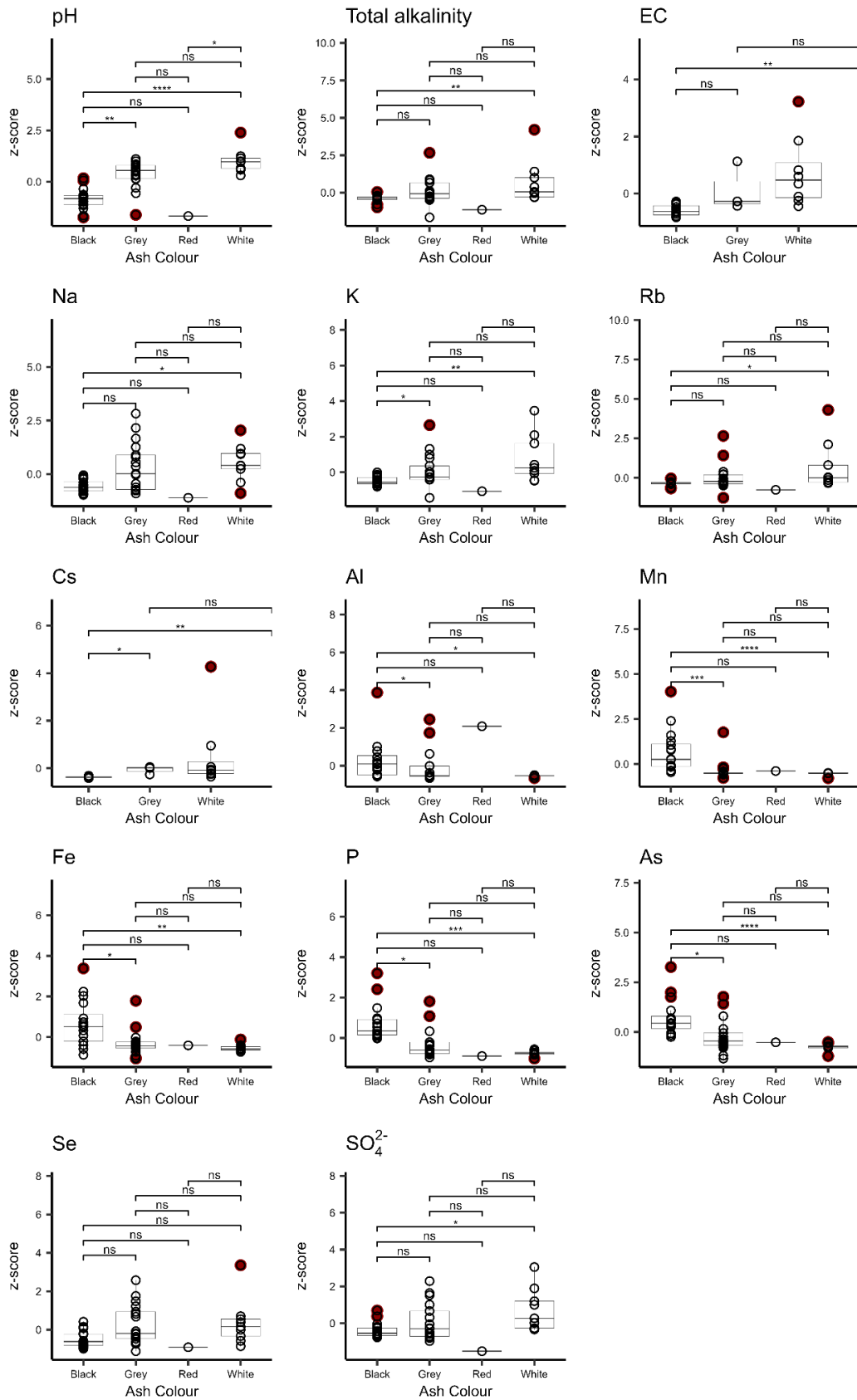
492 We calculated the Ca/Mg ratio for each sample (Figure 4) and found that black ash
493 leachates consistently have a Ca/Mg ratio greater than one (>80% of black ash samples), grey
494 samples have a median Ca/Mg value of less than one, but 35% of samples had a ratio greater
495 than one. While the median Ca/Mg value for white ash is slightly higher than that of grey ash
496 (0.57 as opposed to 0.55 – with an outlier of > 30 000 removed from the white samples), but
497 less variable ($\sigma = 0.266$ as opposed to $\sigma = 2.38$) and just two of nine white ash samples have a
498 Ca/Mg value greater than one. The red ash leachate sample had a ratio comparable to that of
499 black ash.



500

501 **Figure 4** Boxplots of Ca/Mg ratios of ash leachates for all sites by ash colour. The
 502 **dashed red line indicates a Ca/Mg ratio of 1.** Note that two outliers are omitted from
 503 **this plot by the y-axis scaling - one black ash sample with a Ca/Mg value of 11.8, one**
 504 **grey ash sample with a Ca/Mg of ~9.2, and one white ash sample with a value of**
 505 **34067.8, due to very low Mg concentration in that sample.**

506 Ash leachate chemistry has been shown to vary with ash colour, which is itself a
 507 product of combustion completeness. Here, we tested for significant difference in ash
 508 leachate chemistry between ash colours using both the Kruskal-Wallis ranked sum test and
 509 Dunn's test, which makes multiple pairwise comparisons. The results of the Kruskal-Wallis
 510 test showed that there is a significant difference in the pH, total alkalinity, EC, Na, K, Rb, Cs,
 511 Al, Mn, Fe, P, As, Se, and SO_4 (see Table S4 for Kruskal-Wallis p-values). Dunn's test for
 512 multiple comparisons show which ash colour groups are statistically different from one
 513 another. Figure 5 shows boxplots of the z-scores of each variable by ash colour. The results of
 514 Dunn's test are labelled, showing that in general it is only the severity end members (black
 515 and white ashes) which report significantly different concentrations. Boxplots of all variables
 516 by ash colour are found in Figure S4, and a table of mean non-normalised values for each
 517 variable is presented in Table S5.



518

519

520

Figure 5 Boxplots showing z-scores of ash leachate elemental concentrations, electrical conductivity, pH, and alkalinity. The results of Dunn's test are also indicated. *

521 **indicates significance at $\alpha = 0.05$, ** significant at $\alpha = 0.01$, *** significant at $\alpha = 0.001$,**
522 ****** significant at $\alpha = 0.0001$. Red points indicate outliers.**

523 Where black and white ash leachate analytes were significantly different (pH, total
524 alkalinity, EC, Na, K, Rb, Cs, Al, Mn, Fe, P, As, and SO_4), values were higher in black than
525 white ash leachates for Al, Mn, Fe, P, and As, while values were higher in white than black
526 ash leachates for total alkalinity, pH, EC, Na, K, Rb, Cs, and SO_4 . Despite the Kruskal-Wallis
527 test indicating that concentrations of Se were significantly different between different
528 coloured ashes (Table S4), Dunn's Test found that the chemistry of the black, grey, and white
529 ash leachates were statistically similar for these analytes. While in general the differences
530 between the end members (black and white ash) were the most significant, grey and black
531 ashes were significantly different for pH, K, Cs, Al, Mn, Fe, P, and As. There is no evidence
532 of statistical differences between grey and white ashes (Figure 5).

533 **3.1.2 Predictors of ash leachate chemistry**

534 Shapley value regression is used to quantify the influence of predictor variables (see
535 section 2.6). Standardized Shapley regression values were calculated for each of the 27 ash
536 leachate variables and four predictors (ash colour, location, year since the last fire, and the
537 total number of fires), with 95% CIs. Results show that ash colour was the most important
538 predictor for 11 variables (Al, As, Fe, K, Mn, Mo, Ni, P, pH, Rb, and Zn), location was the
539 most influential predictor for 16 variables (Ba, Ca, Cl, Co, Cr, Cu, Mg, Na, Sb, Se, Si, SO_4 ,
540 Sr, total alkalinity, U, and V). Ash colour was the dominant predictor (standardized Shapley
541 value >0.5) for Al, As, Mn, Mo, P, and pH. Location was the dominant predictor for Ba, Ca,
542 Cu, Sb, Se, Si, Sr, U, and V. Neither years since the last fire nor the total number of fires
543 were the dominant predictor for any variables. The highest standardised Shapley value for
544 years since last fire and the total number of fires were 0.288 (Cr) and 0.319 (Mg), although
545 these values were associated with wide CIs (see Table S6 and Figure S5). There is also a high
546 overlap in the 95% CIs for each predictor for many variables, particularly for ash colour and
547 location.

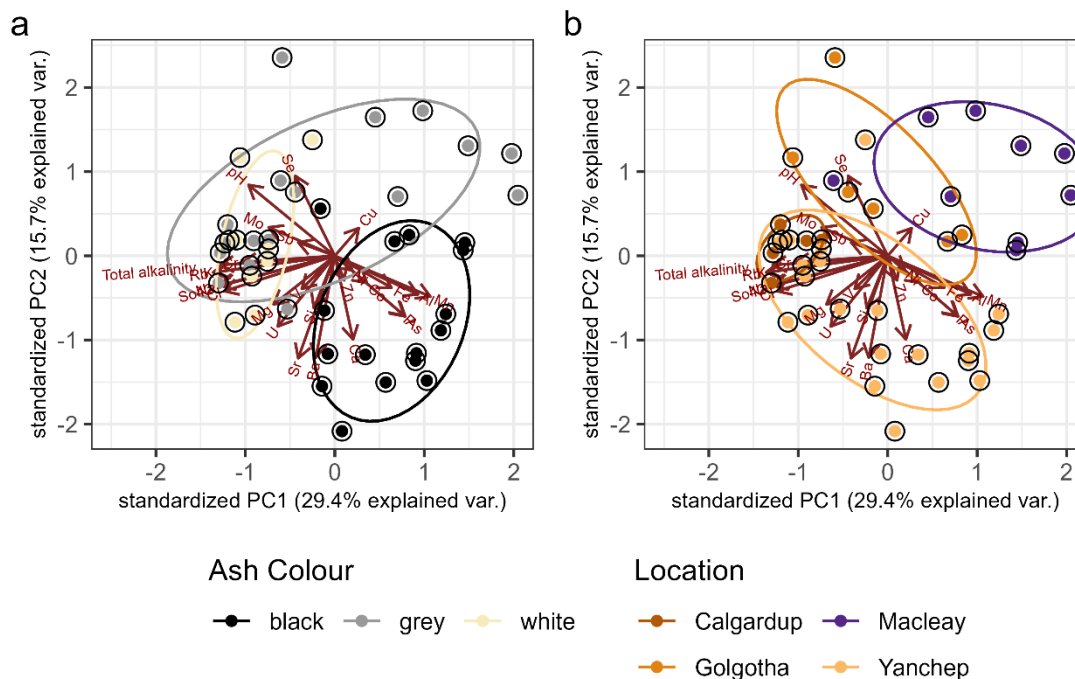
548 PCA was applied to the full ash leachate dataset (Al, As, Ba, Ca, Cl, Co, Cr, Cu, Fe,
549 K, Mg, Mn, Mo, Na, Ni, P, pH, Rb, Sb, Se, Si, SO_4 , Sr, total alkalinity, U, V, and Zn (Table
550 1)). A scree plot (see Figure S6) suggests that while the first three principal components
551 (PCs) contain the most information, the first seven PCs each contain more information than if
552 all PCs explained an equal amount of variance, and so should also be presented. Together the
553 first two PCs account for $\sim 45\%$ of the variance, and $>95\%$ of the variance is described by the
554 first 15 PCs. Loadings can be considered to be important if they contribute more than the
555 average amount of information to the PC. Here, that threshold is ± 0.192 .

556 Table 1 presents the loadings for the first seven PCs. Loadings and a biplot of PC1
557 and PC2 (Figure 6a) shows that black ash samples cluster differently to white and grey ash
558 samples. Variables which load strongly positively on PC1 (Al, Mn) all have higher
559 concentrations in black ash than white ash, while variables which load strongly negatively on
560 PC1 (Cl, Cr, K, Na, pH, SO_4 , Rb, and total alkalinity) are all higher in white ash than black
561 ash, noting that the difference between white and black leachates is not statistically
562 significant for Cl and Cr (Figure 5, Figure S4). The clustering of grey/white versus black ash
563 leachates suggests that burn severity impacts ash leachate geochemistry.

564
565
566

Table 1 Loadings for the first seven PCs from the PCA of ash leachate data. Variables which explain more than one variable's worth of information to the PC (threshold = 0.19) are in bold.

| | PC1 | PC2 | PC3 | PC4 | PC5 | PC6 | PC7 |
|-----------------------------------|---------------|---------------|---------------|---------------|---------------|---------------|---------------|
| Al | 0.218 | -0.147 | 0.162 | -0.115 | 0.089 | -0.291 | 0.194 |
| As | 0.185 | -0.231 | 0.272 | -0.036 | 0.092 | -0.184 | -0.141 |
| Ba | -0.050 | -0.388 | -0.214 | 0.087 | -0.026 | 0.124 | -0.006 |
| Ca | 0.048 | -0.319 | -0.172 | 0.091 | -0.134 | 0.427 | -0.162 |
| Cl | -0.290 | -0.135 | 0.056 | -0.109 | 0.188 | -0.022 | 0.052 |
| Co | 0.084 | -0.103 | 0.264 | 0.150 | -0.416 | 0.154 | -0.016 |
| Cr | -0.242 | -0.024 | 0.026 | -0.281 | -0.168 | -0.237 | 0.009 |
| Cu | 0.063 | 0.105 | 0.208 | -0.043 | -0.363 | 0.305 | 0.457 |
| Fe | 0.148 | -0.121 | -0.214 | -0.231 | 0.106 | 0.227 | 0.484 |
| K | -0.311 | -0.062 | 0.079 | -0.113 | 0.047 | 0.040 | -0.045 |
| Mg | -0.161 | -0.185 | 0.185 | 0.054 | 0.342 | 0.240 | 0.262 |
| Mn | 0.250 | -0.155 | 0.137 | -0.253 | -0.070 | -0.171 | 0.010 |
| Mo | -0.174 | 0.109 | 0.212 | -0.033 | -0.365 | -0.061 | -0.166 |
| Na | -0.302 | -0.112 | 0.022 | -0.113 | 0.111 | -0.065 | 0.088 |
| Ni | 0.046 | -0.055 | 0.409 | -0.188 | -0.055 | 0.296 | -0.064 |
| P | 0.181 | -0.227 | 0.295 | -0.203 | 0.061 | -0.147 | 0.126 |
| pH | -0.226 | 0.271 | -0.076 | 0.067 | -0.176 | -0.137 | 0.147 |
| Rb | -0.319 | -0.063 | 0.016 | -0.107 | -0.035 | -0.038 | 0.067 |
| Sb | -0.096 | 0.051 | 0.371 | 0.258 | 0.144 | 0.254 | -0.090 |
| Se | -0.104 | 0.305 | 0.198 | -0.006 | 0.233 | 0.172 | -0.137 |
| Si | -0.055 | -0.199 | 0.125 | 0.429 | -0.076 | -0.108 | -0.034 |
| SO ₄ | -0.298 | -0.114 | 0.022 | -0.183 | -0.036 | 0.092 | 0.009 |
| Sr | -0.096 | -0.390 | -0.205 | 0.072 | -0.029 | 0.053 | -0.179 |
| Total alkalinity | -0.302 | -0.036 | 0.064 | -0.128 | -0.022 | 0.001 | 0.109 |
| U | -0.149 | -0.269 | 0.021 | 0.095 | -0.369 | -0.220 | 0.102 |
| V | -0.086 | -0.126 | 0.225 | 0.406 | 0.234 | -0.248 | 0.145 |
| Zn | 0.025 | -0.093 | 0.086 | -0.368 | 0.050 | 0.080 | -0.463 |
| Cumulative proportion of variance | 0.29 | 0.45 | 0.58 | 0.65 | 0.72 | 0.77 | 0.81 |



567

568 **Figure 6 Biplots of standardised scores from PCA of ash leachate samples. 6a presents**
 569 **PC1 plotted against PC2, with ash colour shown as both clusters and the point colour.**
 570 **6b also shows PC1 plotted against PC2, with sample location indicated by point colour**
 571 **and clustering.**

572 Similarly, there is clear clustering of points by location, with samples from southwest
 573 western Australia and samples from southeastern Australia having little overlap in a biplot of
 574 PC1 and PC2 scores (Figure 6b), although it should be noted that the majority of Macleay
 575 samples were grey ashes. When samples are grouped by the number of years since the last
 576 fire (two groupings applied: samples below the median (14 years) or equal to and above the
 577 median), the samples clearly cluster, with sites burned less recently having more negative
 578 scores for PC2, while sites which burned more recently having more positive PC2 scores (see
 579 Figure S7). Biplots of the first three PCs for the total number of fires shows no distinct
 580 clustering (see Figure S8).

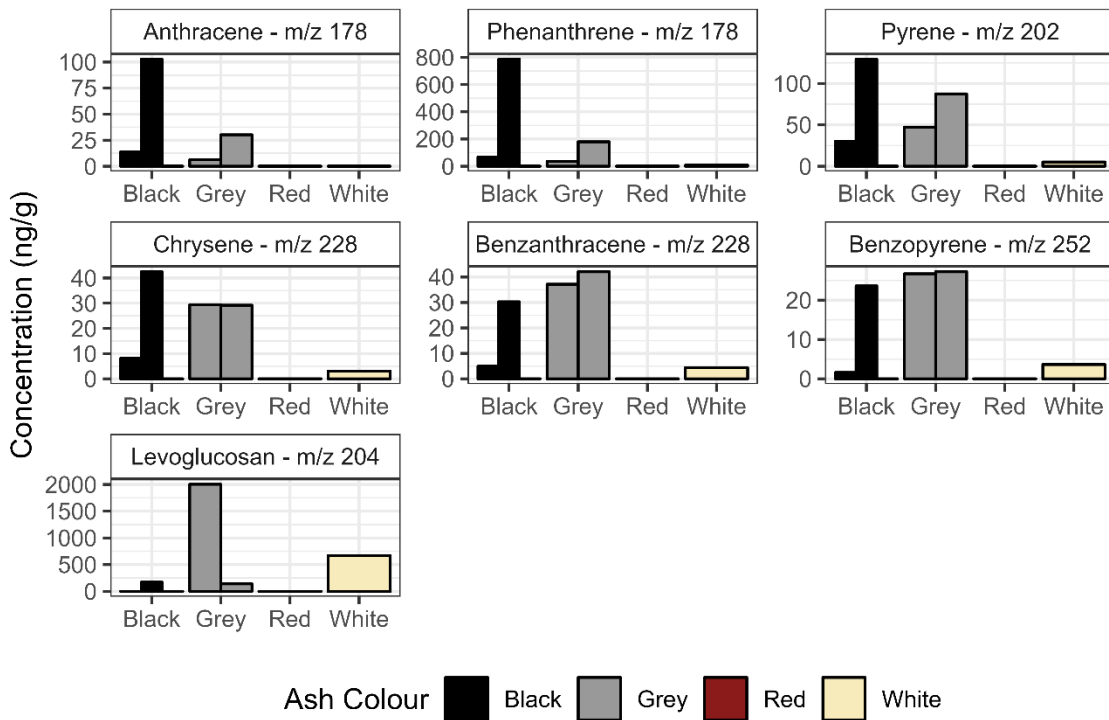
581 3.1.3 Ash biomarkers

582 Thirteen samples from four locations (Golgotha Cave, Calgardup Cave, Macleay, and
 583 Yanchep) were analysed, with six PAHs (Phenanthrene, Anthracene, Pyrene, Chrysene,
 584 Benzanthracene, and Benzopyrene) and levoglucosan detected. Samples from Calgardup
 585 Cave and Macleay had no measurable PAHs or levoglucosan, and samples from Yanchep had
 586 no measurable PAHs, and concentrations of levoglucosan were low (see Table S7). As such,
 587 only ash samples from Golgotha Cave are presented here. Concentrations are normalised to
 588 the dry weight of ash.

589 In general, total concentrations of the low molecular weight compounds (Anthracene,
 590 Phenanthrene, and Pyrene) were higher than for higher molecular weight PAHs (Chrysene,
 591 Benzanthracene, and Benzopyrene). PAH concentrations were generally higher in black and
 592 grey than white ash samples, particularly in the lowest molecular weight compounds, noting
 593 however that the variability for the black ash leachates is high for each PAH (Figure 7 and

594 Table S7), and that one black sample (Golgotha_6) had no measurable PAHs (Table S7). No
595 PAHs were found in the red ash sample.

596



597

598 **Figure 7 Concentrations of PAHs and levoglucosan, by ash colour. PAHs are arranged**
599 **by molecular weight. Note that the scale of the y-axis is different for each plot.**

600 Levoglucosan had a maximum concentration of 2.0 $\mu\text{g/g}$, and a mean concentration of
601 4.3 $\mu\text{g/g}$ (Figure 7, Table S7). Three (two black and one red) of the seven ash samples
602 contained no measurable levoglucosan (see Table S7). Of the four Golgotha Cave samples
603 with measurable concentrations, grey and white samples generally had higher concentrations
604 than black samples (Figure 7).

605 3.2 Soil

606 Standardised Shapley regression values for 17 measured variables and four predictors
607 (location, the number of years since the last fire, the total number of fires, and the sample
608 depth) showed that location had the most explanatory power for all variables in soil leachates
609 (see Table S8). There was no overlap in the 95% CIs between location and the other
610 predictors for any analyte except Si, where CIs for depth, years since last fire, and total
611 number of fires slightly overlapped with those for location (see Table S8 and Figure S9). This
612 suggests that for most variables, sample location clearly has the greatest influence.

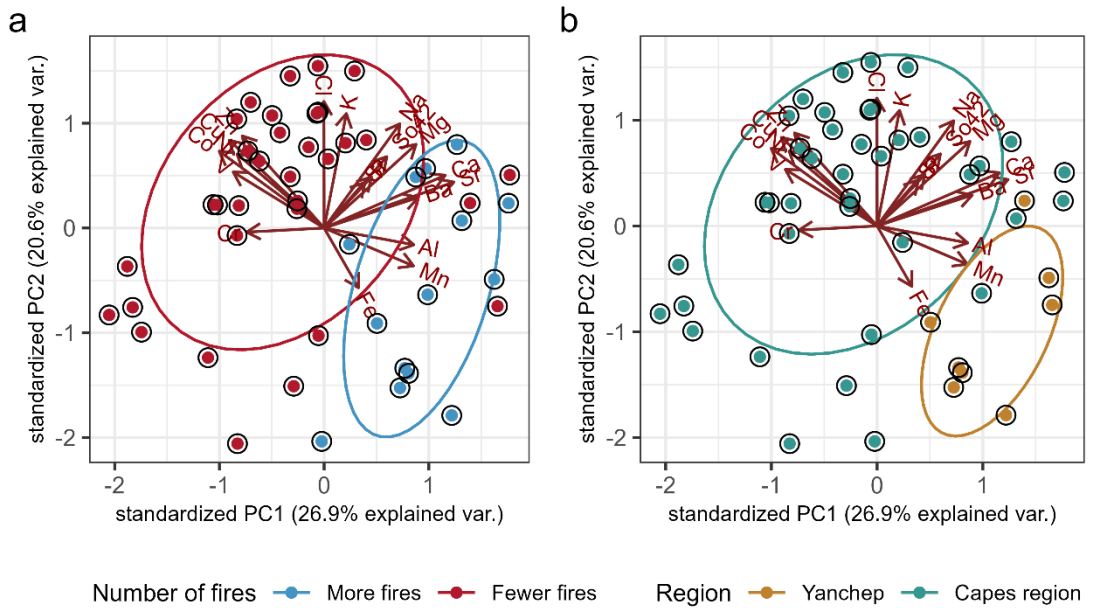
613 PCA was repeated on the soil leachates, using the same variables as for the PCA of
614 ash leachates in Section 3.1, but with the exclusion of As, Mo, pH, Rb, Sb, Se, total alkalinity,
615 and U due to missing data (Table 2). A scree plot (see Figure S10) suggests that while the first
616 two PCs explain the most variance, the first five PCs each explain an above-average
617 proportion of the variance, and should be presented. Together, the first two PCs explain ~48%
618 of the variance, and >95% of the variance is explained by the first 13 PCs. Following Section
619 3.1, the threshold for loading 'importance' is ± 0.229 . Table 2 presents the loadings for the
620 first five PCs. Variables which load strongly positively on PC1 (Al, Ba, Ca, Mg, Mn, Sr) are
621 all variables which tend to be higher in the Yanchep region than the Capes region, and which

622 are higher at sites which have experienced more fires. Similarly, the variables which load
 623 strongly negatively on PC1 (Co, Cu, Ni, and V) are all lower for samples from the Yanchep
 624 region, and for samples which have experienced more fires. This is illustrated in a biplot of
 625 PC1 and PC2 (Figure 8).

626 Cl, Co, Cu, K, Mg, Na, Ni, and Zn load strongly positively on PC2, while no variable
 627 loads strongly negatively. A biplot of PC1 and PC2 with scores coloured by the distance to
 628 the coast (Figure 9) suggests that PC2 reflects proximity to the coast, with higher Cl, K, Mg,
 629 and Na in samples with higher exposure to sea spray (Davies and Crosbie, 2018).

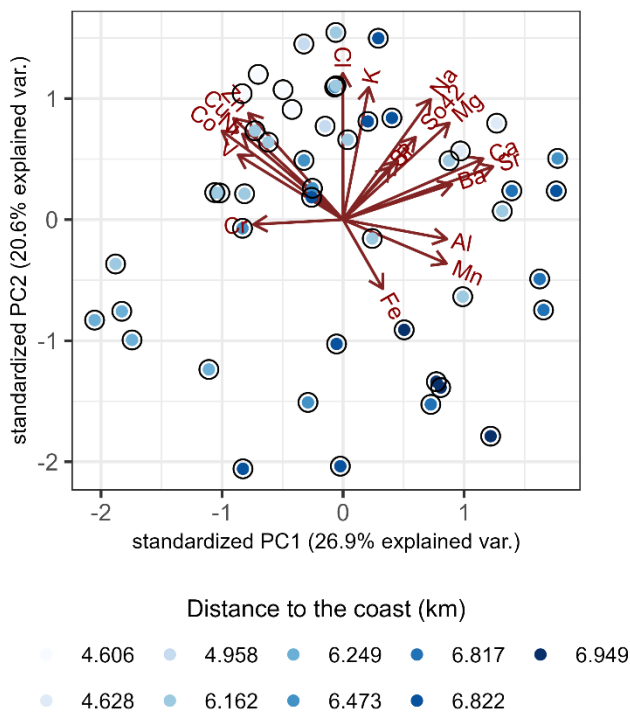
630 **Table 2 Loadings for the first five PCs of soil leachate chemistry. Bold indicates which**
 631 **variables have a greater proportion of influence on the PC (threshold of ± 0.229)**

| | PC1 | PC2 | PC3 | PC4 | PC5 |
|-----------------------------------|---------------|--------------|---------------|---------------|---------------|
| Al | 0.250 | -0.053 | -0.315 | -0.078 | -0.496 |
| Ba | 0.263 | 0.097 | 0.137 | 0.309 | -0.010 |
| Ca | 0.338 | 0.168 | 0.198 | 0.178 | -0.238 |
| Cl | -0.001 | 0.403 | -0.126 | -0.300 | 0.042 |
| Co | -0.292 | 0.245 | -0.130 | 0.086 | -0.080 |
| Cr | -0.216 | -0.013 | -0.396 | 0.044 | -0.407 |
| Cu | -0.265 | 0.279 | 0.071 | 0.079 | 0.039 |
| Fe | 0.096 | -0.190 | -0.512 | 0.123 | -0.145 |
| K | 0.062 | 0.365 | -0.355 | 0.061 | 0.118 |
| Mg | 0.256 | 0.267 | 0.017 | 0.235 | -0.224 |
| Mn | 0.249 | -0.121 | -0.238 | -0.054 | 0.333 |
| Na | 0.211 | 0.332 | -0.026 | -0.344 | 0.107 |
| Ni | -0.243 | 0.236 | 0.005 | 0.262 | 0.073 |
| P | 0.132 | 0.163 | -0.204 | 0.434 | 0.264 |
| Si | 0.114 | 0.145 | -0.301 | -0.010 | 0.389 |
| SO ₄ | 0.175 | 0.227 | 0.060 | -0.499 | -0.106 |
| Sr | 0.362 | 0.146 | 0.203 | 0.120 | -0.156 |
| V | -0.253 | 0.178 | -0.058 | -0.130 | -0.166 |
| Zn | -0.228 | 0.293 | 0.149 | 0.166 | -0.157 |
| Cumulative proportion of variance | 0.269 | 0.476 | 0.585 | 0.69 | 0.746 |



633

634 **Figure 8 A biplot of soil leachate PCA PC1 and PC2, with scores coloured by the**
 635 **number of fires (a) and the region (b).**



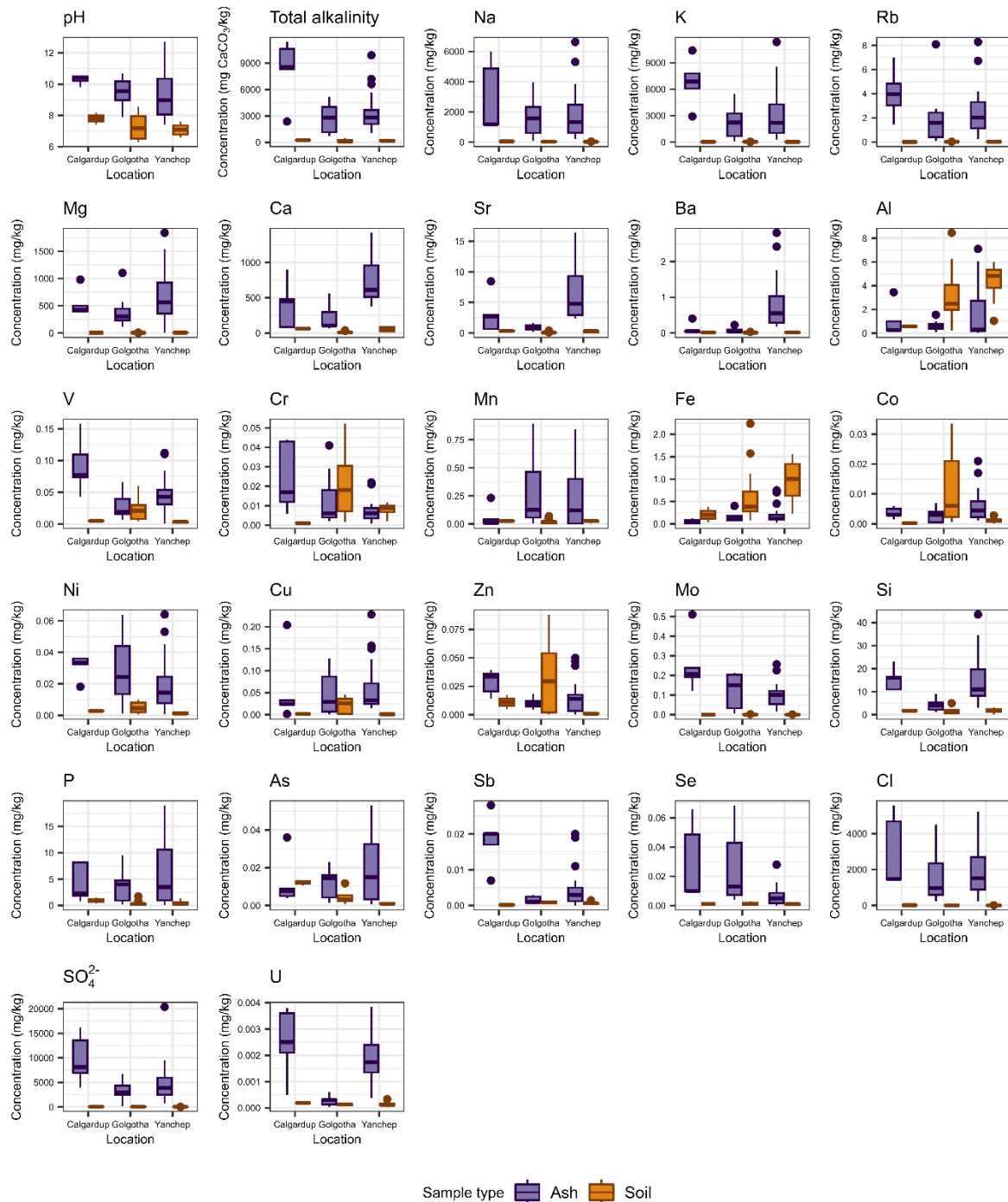
636

637 **Figure 9 A biplot of soil PCA PC1 and PC2, with scores coloured by the distance from**
 638 **sample location to the coast (in km)**

639 Figure 10 compares ash and soil leachate data for sites where both ashes and soils
 640 were collected (Calgardup Cave, Golgotha Cave, and Yanchep). Ash leachates have higher

641 pH and alkalinity than soil leachates for all sites. Elemental concentrations are generally
642 higher in ash leachates than soil leachates at two or more sites for all elements barring Fe, Al,
643 and Cr. Concentrations of Fe are higher in soil leachates than in ash leachates at all sites.
644 Concentrations of Al and Cr in soil leachates either exceed or are comparable to ash leachates
645 (except for Calgardup Cave, where soil leachate Cr concentrations are very low).
646 Concentrations of Na, K, Rb, Mg, Ca, Sr, Ni, Mo, P, Se, Cl, and SO₄ in ash leachates clearly
647 exceed concentrations in soil leachates at all sites. Mn concentrations are generally higher in
648 ash leachates at Golgotha Cave and Yanchep, but are comparable to soil leachates at
649 Calgardup Cave. Concentrations of Ba, V, Co, Cu, Zn, Si, Sb, and U are higher in ash
650 leachates than in soil leachates for Calgardup Cave and Yanchep samples, but are comparable
651 in Golgotha Cave samples. A table of median soil leachate concentrations is found in Table
652 S9. Concentrations of Al, Cl, Cr, and Fe were higher in leachates of deeper soils than in
653 shallower soils (see Table S10).

654



655

656 **Figure 10** Boxplots of ash leachate (purple) and soil leachate (brown) chemistry for each
 657 site where both soils and ashes were collected (Calgardup Cave, Golgotha Cave, and
 658 Yancheop.

659 **4 Discussion**

660 Overall, our results shows that inorganic ash leachate chemistry varies with burn
 661 severity (as indicated by ash colour) and location, and that the past fire history (i.e., the total
 662 number of fires for each site, and the number of years since the last fire for each site), had a
 663 more limited effect on ash leachate chemistry. Ash leachate pyrogenic biomarker results were
 664 variable, and the relationship between ash colour and biomarker concentrations was not clear.
 665 Soil leachate chemistry was shown to vary between sites, and as for ash leachates, the fire

666 history had minimal impact on soil leachate chemistry. Ash leachates were generally shown
667 to be more enriched in a range of analytes, compared to soil leachates.

668 **4.1 Ash and soil leachate chemistry**

669 4.1.1 General ash leachate chemistry

670 Of the 29 measured variables which met the threshold for inclusion ($\geq 25\%$ of samples
671 $> \text{LOD}$), SO_4 , K, Cl, Na, and Ca were the most abundant elements in ash leachates, while U,
672 Sb, Co, Cr, and Se were the least abundant elements. The elevated SO_4 , K, Cl, Na values in
673 ash leachates are likely due to higher exposure of vegetation to sea spray, with all Western
674 Australian ash samples collected within 8 km of the coast and downstream of the dominant
675 southwesterly winds. This is also reflected in the soil leachate data, where PC2 reflected sea
676 spray inputs and where the most abundant elements are Na, Cl, K, Ca, and SO_4 (Figure 10).

677 Our analyses of ash leachates from karstified limestone environments found Na to be
678 the most abundant element, followed by Ca and Mg. These findings are broadly consistent
679 with a recent global analysis of wildfire ash leachate data, which showed Na, Ca, and Mg to
680 also be the most abundant (Ca $>$ Na $>$ Mg) (Sánchez-García et al., 2023). The predominance
681 of Na in our samples again likely reflects the strong marine influence at our southwest
682 Australian sites. The global analysis also showed that wildfire ash leachates were least
683 abundant in F, Mn, and Fe, which is also in broad agreement with our results. Ash leachate
684 concentrations presented here were generally higher than the ‘temperate eucalypt forest’ ash
685 leachates from southeast Australian forests reported in Sánchez-García et al. (2023).
686 However, Fe and Mn are an exception; our results show that these elements were both lower
687 in concentration and outside the range of data presented by Sánchez-García et al. (2023).

688 **4.1.2 Ash leachate chemistry changes with burn severity**

689 Several studies have suggested that there is a relationship between combustion
690 completeness and the Ca/Mg ratio, and a ratio < 1 is thought to indicate severe burning
691 (Marion et al., 1991; Úbeda et al., 2009). Broadly, the results support the hypothesis that a
692 Ca/Mg ratio < 1 indicates severe burning, particularly for the combustion end-members (black
693 and white ash), but considerable spread in the data remains. This uncertainty is consistent
694 with other studies. Úbeda et al. (2009) in a laboratory study of *Quercus suber* ash found that
695 the relationship between the Ca/Mg ratio and combustion completeness only held for one site.
696 While this ratio would require Ca concentrations to decrease with burn severity and Mg
697 concentrations to increase with burn severity (or for one of these to not change with burn
698 severity), the Kruskal-Wallis test found no statistical difference in the concentrations of these
699 analytes between ash colours. However, a qualitative assessment of the data (see Figure S4)
700 shows that in general, Ca concentrations are lower in white leachates than black ash
701 leachates, while Mg concentrations are higher in white ash leachates. The lack of statistical
702 difference between the concentrations of these analytes by combustion completeness is
703 consistent with the literature, where they are generally reported to behave similarly (Balfour
704 and Woods, 2013; Miotliński et al., 2023; Pereira et al., 2012; Úbeda et al., 2009), although
705 Sánchez-García et al. (2023) reported that Ca concentrations were higher in ash leachates
706 produced from severe burning, and that Mg concentrations did not vary with burn severity.
707 The predominantly negative charge imbalances of the leachates also support the hypothesis
708 that black ashes are less-combusted than white ashes. This was attributed to higher levels of
709 organic matter in black ashes, which can contribute negative ions that are unaccounted for by
710 our charge balance calculations.

711 Our hypothesis that ash leachate chemistry will change with burn severity, is
712 supported by the Kruskal-Wallis rank sum test and post-hoc Dunn’s test, which showed that

713 pH, total alkalinity, EC, Cs, Rb, K, Na, and SO₄ increased with combustion completeness,
714 while As, Fe, Mn, P, Al, and Zn decreased with combustion completeness. The Shapley value
715 regression and PCA also indicated that ash colour (representing combustion completeness) is
716 a key control on ash leachate chemistry. Note that in both Dunn's test and the PCA, there is
717 little statistical difference between black and grey or grey and white ashes in any variable
718 aside from K, where black ash leachates were significantly different from both grey and white
719 ash leachates (Figure 6a). This suggests that it is only the severity end-members (more
720 completely burned versus less completely burned) that can be distinguished in these analyses.
721 We found no statistically significant difference in the water extractable proportion of Se, Ba,
722 Ca, Sr, V, Sb, Mo, Cu, Mg, U, Cl, Cr, Ni, Si or Co by ash colour.

723 A comparison of our results with the literature is presented in Text S5. While a review
724 of the literature broadly indicates that ash chemistry changes with burn severity, there is
725 considerable heterogeneity of results, suggesting that there is a spatial and perhaps
726 methodological influence on how ash geochemistry changes with burn severity. There is
727 better agreement between studies of the water-extractable component of ash leachates (e.g.
728 Burton et al., 2016; Miotliński et al., 2023; Pereira et al., 2012; Quintana et al., 2007;
729 Sánchez-García et al., 2023; Úbeda et al., 2009), with acid-digested samples tending to be
730 less consistent. In general, our results show strong agreement with Miotliński et al. (2023),
731 for leachate data from combustion simulation experiments conducted on soils and vegetation
732 litter from southwestern Western Australia, see Table S5.1 in Text S5.

733 If volatilization temperature was the sole control on element concentration with burn
734 severity, we would expect to see concentrations of elements with high volatilization
735 temperatures (e.g. Mn, Al, Zn, K, P, Cu, Mg, Ca and Na, which all volatilize at >700 °C (see
736 summary figures in Campbell et al. (2023) and Bodí et al. (2014)) in greater relative
737 proportions in white ashes than in black ash. This is true for Na and K which are higher in
738 white ash leachates than in black ash leachates, but Mn, Al, P, and Zn are higher in black ash
739 leachates than in white, and Cu, Mg, and Ca concentrations do not vary significantly with ash
740 colour. Volatilisation temperatures reported in the literature are largely based on empirical
741 combustion studies with varying experimental designs. Additional factors which may impact
742 ash leachate chemistry beyond volatilisation temperature include combustion completeness
743 (which can be independent of fire temperature), that the solubility of some metals changes
744 with pH, and that some metals are likely to be present in complexes with organic matter
745 (which is typically higher in incompletely combusted black ashes; Quill et al., 2010).

746 Levoglucosan is thought to form at burn temperatures between 150-350 °C (Kuo et
747 al., 2008). Kuo et al. (2008) found that maximum levoglucosan yield in laboratory-produced
748 black char occurred at 250 °C, and was independent of combustion duration. In results
749 presented here, levoglucosan is highest in grey and white ashes, noting both the small sample
750 sizes and that the spread of the grey data is high, and that while the highest concentration
751 levoglucosan was found in a grey ash sample, the lowest non-zero concentration was also a
752 grey ash sample. This may indicate that grey ash samples are heterogeneous. Alternatively,
753 the difference between the two grey ash samples may be because levoglucosan production is
754 independent of burn time (Kuo et al., 2008), and the grey sample with higher levoglucosan
755 concentration may have been produced by long slow smouldering rather than hot fire.

756 Laboratory and field experiments have shown that low molecular weight PAHs tend
757 to be more abundant in post-fire soils and burn residues after fires at low-to-moderate
758 temperatures (Kim et al., 2011; Karp et al., 2020; Rey-Salgueiro et al., 2018; Simon et al.,
759 2016), with lower concentrations found in laboratory residues at very low (<300 °C) and very
760 high (>600 °C) temperatures (Karp et al., 2020). In wildfire ashes, summed PAHs have been

761 shown to be higher in black than in white ashes (Chen et al., 2018). In results presented here,
762 PAH concentrations are generally higher in the lower molecular weight PAHs for all ash
763 colours (Figure 7 and Table S7). Summed PAHs are also generally higher in black and grey
764 ashes (see Figure S4.1 in Text S4), although there is significant variability in concentrations
765 of the black ash samples (noting that only one each of red and white ashes are presented
766 here). Higher concentrations of PAHs in black and grey ashes is to be expected, as at high
767 temperatures PAHs may be completely combusted, or incorporated into larger aromatic
768 compounds (Karp et al., 2020).

769 **4.1.3 Ash and soil leachate chemistry varies among sites**

770 Ash leachate chemistry varied between sites. Shapley value regression showed that
771 for 16 variables (Ba, Ca, Cl, Co, Cr, Cu, Mg, Na, Sb, Se, Si, SO₄, Sr, total alkalinity, U, and
772 V) location had more influence on ash leachate chemistry than ash colour. The second-most
773 important predictor (above the threshold of 0.25, which indicates if a predictor explains more
774 than its share of variance) was ash colour for Ba, Ca, Cl, Co, Cu, Na, Se, Si, SO₄, and total
775 alkalinity. For Cr, years since the last fire was the second-most important predictor, while for
776 Mg, the total number of fires was the second-most important predictor. The importance of
777 location is also shown in the PCA, with ash leachates from different locations clustering
778 differently, with the difference most obvious between southeast and southwest Australian
779 samples. While there has been limited research on ashes from multiple sites, Úbeda et al.
780 (2009) showed that in laboratory conditions, ash produced from *Quercus suber* from two
781 different sites had distinctly different physical and chemical compositions. Sánchez-García et
782 al. (2023) found that ashes from different sites clustered differently, although they attributed
783 differences between the clusters to delays in sampling post-fire (with samples being rained
784 on, or loss of the finer particles by wind) and to legacy contamination from industrial activity.

785 Time since sampling may have contributed to differences between Macleay ashes and
786 the southwest Australian ashes, as the Macleay site was inaccessible due to the long duration
787 of the Carrai East Fire. Approximately a month elapsed between the extinguishing of the fire
788 in January 2020 and sampling in early February 2020, although due to the large size of the
789 Carrai East Fire it is possible that the area that was sampled had extinguished much earlier
790 than other parts of the fire. Both Golgotha Cave and Yanchep ashes were collected
791 approximately one month after the respective wildfires, while Calgardup Cave ashes were
792 collected one day after the prescribed burn.

793 Location was the most important predictor for soil leachates, as indicated by Shapley
794 value regression and PCA results. Sub-plot-scale heterogeneity in soils has been well-
795 documented (Campbell, 1979; Harris, 1915). The Shapley value regression showed that
796 location was the dominant predictor for all variables. As for ash leachates, a standardised
797 Shapley value >0.25 indicates that a predictor explains more than its share of variance if all
798 predictors had equal predictive power. Unlike for ash leachate results, there are very few
799 variables where the second-most important predictor exceeds this threshold (Cl and V), and
800 for both variables the second-most important predictor was the total number of fires. Both
801 PC1 and PC2 described some aspect of soil sample location, with PC1 perhaps conflating
802 total number of fires and location, while elements which loaded strongly positively on PC2
803 were related to distance from the coast via sea spray inputs.

804 **4.1.4 Limited evidence of memory of previous fires in ash and soil leachates**

805 Neither the total number of fires nor the number of years since the last fire (both
806 describing fire history) explained a large proportion of the variance in ash leachate chemistry,
807 although PCA analysis of ash leachates showed that PC2 may describe the number of years

808 since the last fire, with sites which burned more recently loading positively on PC2, and sites
809 which burned less recently loading negatively on PC2. Similarly, sites which had experienced
810 more fires loaded positively on PC2, while sites which had experienced fewer fires loaded
811 negatively on PC2, although the clustering is not as distinct as for the number of years since
812 the last fire. This is reflected in the Shapley value regression, where the number of years
813 since the last fire tends to be a more important predictor than the total number of fires
814 (although less important than either ash colour or location). Shapley value regression showed
815 that the number of years since the last fire had a sizable impact on Cr and SO₄ concentrations,
816 while the total number of fires impacted Mg and Ni. This is consistent with Miotliński et al.
817 (2023) who found higher concentrations in ashes produced from leaf litter and soil sampled
818 from a site which had burned recently (2 months) than from a site burned less recently (4.5
819 years). That the effect appears to be tertiary to location and burn severity here may be
820 explained by the much longer interval between the penultimate fire in results presented here.

821 As for ash leachates, neither the number of years since the last fire nor the total
822 number of fires explained a large proportion of the variance in soil leachate chemistry,
823 although PC1 may reflect the total number of fires (although this is potentially a confounding
824 effect produced by correlation between location and the total number of fires, with Yanchep
825 recording more fires than sites in the Capes region). Unlike for ash leachates, Shapley value
826 regression of soil leachates suggests that the total number of fires has more impact on soil
827 leachate chemistry than the number of years since the last fire, although only two variables
828 (Cl and V) had standardised Shapley values >0.25.

829 **4.2 Implications for palaeofire research**

830 Past fire activity can be reconstructed using inorganic and organic proxies preserved
831 in environmental archives such as soils, sediments, or ice cores. In recent years speleothems
832 have been used to reconstruct past fire activity in Australia and North America (Argiriadis et
833 al., 2019, 2023; Homann et al., 2023, 2022; McDonough et al., 2022). Fire sensitive
834 stalagmite proxies include trace and minor elements and nutrients, calcite $\delta^{18}\text{O}$, and fire-
835 sensitive biomarkers. Trace and minor elements and biomarkers are thought to reach
836 stalagmites after originating in burned vegetation and soil and being carried by infiltrating
837 waters through the vadose zone before being sequestered in the growing stalagmites.

838 Ash and soil leachates confirm that the inorganic fire signal is likely to be originating
839 from the ash, as concentrations of many analytes (including Na, K, Rb, Ba, V, Mn, Co, Ni,
840 Cu, Mo, Si, P, As, Sb, Se, Cl, SO₄) are generally higher in ash leachates than in soil leachates,
841 although there is some variability by location. Additionally, many elements vary with ash
842 colour (itself a proxy for burn severity) suggesting that burn severity as well as fire frequency
843 may be recorded by speleothems, as first suggested by McDonough et al. (2022). While some
844 analytes are both higher in ash leachates than in soil leachates and vary with burn severity
845 (e.g. Na, K, Rb, Mn, P, As, and SO₄) not all may be of sufficient concentration to be
846 detectable by LA-ICP-MS or synchrotron X-ray Fluorescence Microscopy, the standard
847 methods to measure stalagmite trace element.

848 The pyrogenic biomarkers analysed here (six PAHs and levoglucosan) were in low
849 abundance in the majority of ash leachate samples (see Table S7 for abundances). This may
850 have been due to degradation *ex situ* when stored at laboratory temperatures (Douglas et al.,
851 2018; Rost et al., 2002). The samples that had measurable biomarkers were collected and
852 analysed within two months, a long enough delay that some degradation can be expected to
853 have occurred (Douglas et al., 2018), although repeat analyses of samples presented here
854 suggests that degradation may be non-linear or secondary to sample heterogeneity (see Figure
855 S4.2 in Text S4). Douglas et al. (2018) showed that Chrysene and Pyrene were robust to

856 degradation under ambient temperatures. Concentrations of both Chrysene and Pyrene in
857 samples presented here were low, and there was no clear trend by ash colour for either
858 compound, although in general black and grey ashes had higher concentrations of both
859 compounds. Considering all PAHs presented here, concentrations tended to be higher in the
860 lower molecular weight compounds, and summed concentrations were highest in black and
861 grey ash samples. This is consistent with both laboratory studies and analysis of wildfire
862 ashes, which have demonstrated that highest PAH concentrations from between 400-600 °C
863 (Karp et al., 2020), and which have shown total concentrations are higher in black ashes than
864 in white ashes (Chen et al., 2018).

865 Anhydrosugars (including levoglucosan) are reactive and soluble. In open fires, they
866 may appear in all phases (as gas, particles, or in charcoal) (Suciu et al., 2019). Anhydrosugars
867 are released in greatest quantities at ~300 °C (Shafizadeh et al., 1979; Suciu et al., 2019),
868 although a second peak may be observed at 600 °C due to the depolymerisation of polymeric
869 products formed from the thermal conversion of water-soluble compounds (Suciu et al.,
870 2019, p. 213). Suciu et al. (2019) suggest that it is the reaction of these high-temperature
871 anhydrosugars, with aromatic substances which may result in anhydrosugars forming in char.
872 While there is no clear trend in levoglucosan concentration by ash colour, in general
873 concentrations are higher in grey and white ash samples than in black ash samples. As the
874 chemical structure of anhydrosugars means they bond well with chelating metals (e.g. Fe and
875 Al; Suciu et al., 2019), we could have expected that the samples with the highest
876 levoglucosan concentrations would also have high concentrations of Fe and Al. Instead, we
877 find that of those seven samples, the highest concentrations of levoglucosan are found in the
878 sample with the third highest Fe concentrations and the lowest Al concentrations (of the
879 seven Golgotha Cave ash samples presented in section 3.1.3). As for the PAHs, a larger
880 sample size with reduced opportunity for sample degradation is needed to be able to draw
881 stronger conclusions about the use of levoglucosan as a speleothem palaeofire proxy.

882 That biomarker concentrations may degrade in both collected samples (Douglas et al.,
883 2018; Rost et al., 2002), and *in situ* (Kim et al., 2011; Simon et al., 2016; Yang et al., 2010)
884 should be considered when interpreting them as proxies for past fire. For example, in
885 southwest Western Australia, the bushfire season peaks in summer and autumn. Dripwater
886 monitoring at Golgotha Cave has shown that activation of fractures (and so potentially more
887 efficient transport of the surface fire signal) is generally enhanced when soil stores are
888 saturated (Priestley et al., 2023), which may be months after the fire season has finished. This
889 suggests that where biomarkers are incorporated in speleothems, they may have been
890 degraded prior to inclusion. Additionally, that low molecular weight PAHs are generally more
891 abundant than high molecular weight PAHs, and that total PAH concentrations are higher in
892 black and grey ashes than in white ashes both suggest that PAH-derived records of past fires
893 may be biased towards less-severe burns. Homann et al. (2023) found that high molecular
894 weight PAHs were often <LOD in a Mexican speleothem. They attributed this to filtering of
895 high molecular weight PAHs by overlying soils and epikarst, as earlier suggested by Perrette
896 et al. (2013). Our results suggest that, if speleothem PAHs are derived from the leaching of
897 deposited ashes, high molecular weight PAHs and PAHs sourced from more severe fires are
898 unlikely to be incorporated, as initial concentrations of both are low, and karst processes are
899 likely to further dilute them. While results presented here will be useful for the interpretation
900 of pyrogenic biomarkers in speleothems, more research is needed to better understand the
901 transport and deposition of pyrogenic biomarkers in karst systems.

902 **4.3 Implications for surface and groundwaters**

903 The impact of wildfire on surface waters has been well-documented, and elevated
904 concentrations of contaminants are commonly seen (Beyene et al., 2023; Hickenbottom et al.,

905 2023), along with increased turbidity (Chen and Chang, 2022; Emmerton et al., 2020) and
906 changes in pH (Costa et al., 2014; Granath et al., 2021), all of which pose risk to both natural
907 and human systems. Karst systems make up 7-12% of the terrestrial earth surface, and ~25%
908 of the world's population rely on karst aquifers for their water supply (Ford and Williams,
909 2007; Hartmann et al., 2014). While groundwaters are generally thought to be less susceptible
910 to contamination than surface waters (Reberski et al., 2022), contamination of karst
911 groundwaters is a known concern (Vilhar et al., 2022). Contaminants may be both autogenic
912 and allogenic, occurring as both point-source and diffuse sources (Ford and Williams, 2007).
913 Karst aquifers are susceptible to pollution because they very efficiently transport
914 contaminants and they have limited capacity to filter them (Ford and Williams, 2007;
915 Sasowsky, 2000). Karst aquifers have been contaminated by a range of pollutants such as
916 fertilisers, pesticides, pharmaceuticals, microplastics, effluent, and urban and agricultural
917 runoff (Jiménez-Sánchez et al., 2008; Reberski et al., 2022; Panno et al., 2019). That karst
918 aquifers may be more susceptible to contamination than non-karst aquifers is demonstrated
919 by Reberski et al. (2022), who in a review of fifty studies of anthropogenic contaminants in
920 karst aquifers showed that while concentrations of anthropogenic contaminants were lower in
921 karst aquifers than in surface waters, karst aquifers had higher concentrations of those
922 contaminants than other aquifers.

923 There has been limited research on the impact of fire as a contaminant source in karst
924 aquifers, but land clearing and fire are both thought to result in heightened nutrient loading in
925 karst systems (Gillieson and Thurgate, 1999). In the karst vadose zone, the geochemical
926 response to fires in dripwater is variable, and appears to depend on both the burn severity and
927 the cave depth (Coleborn et al., 2019, 2018; Nagra et al., 2016; Treble et al., 2016). Fires
928 have also been implicated in enhanced recharge in the vadose zone, through heat-induced
929 fracturing of the host rock (McDonough et al., 2022; Meng et al., 2020; Wu and Wang, 2012).
930 McDonough et al. (2022) attributed enhanced organic matter in a speleothem to increased
931 fracture flow following a severe bushfire. Fires have also been implicated in reduced
932 infiltration in karst due to sealing of the epikarst (the uppermost layer of the karst; Holland,
933 1994), although there has been little reporting of this effect. Metals are listed as a key karst
934 contaminant (Vesper et al., 2003), and results presented here show that post-fire ashes may be
935 a point-source of metal contamination, at concentrations higher than normally found in soils.
936 Concentrations of key potential contaminants (As, Ba, Co, Cu, Mn, Mo, Ni, Sn, V, Zn, P, S,
937 SO₄, Phenanthrene, Anthracene, Pyrene, and Benzopyrene) in both ash and soil leachates are
938 generally lower than the Western Australian Ecological Investigation Levels (Department of
939 Environment and Conservation, 2010; see Table S11), with the exception of S and SO₄, which
940 both exceed the ecological investigation levels. While concentrations are generally low, ash
941 leachate concentrations are much higher than soil leachate concentrations (Table S11), and it
942 is unclear how flushes these potential contaminants might impact the karst environment,
943 including both fragile cave ecosystems and water resources. Further investigation is required
944 at scales ranging from the cave to the catchment to determine whether ash inputs are a
945 significant contamination source for karst aquifers. Since climate change is likely to strain
946 global water resources, and since karst aquifers make such a large contribution to global
947 water resources, understanding how best to minimise their contamination needed to ensure
948 future water security.

949 **5 Conclusion**

950 Ashes from both wild and prescribed fires are sources of both contaminants and
951 potential fire proxies for palaeoenvironmental research. In our analyses of ash leachates from
952 ashes collected in both southwest and southeast Australia, we found that ash leachate
953 inorganic chemistry primarily varies with ash colour (which is an indicator of burn severity)

954 and location. Statistical difference in inorganic analyte concentration by ash colour was
955 mainly found between the ash colour severity ‘end-members’ (i.e. black vs white ashes). This
956 suggests that palaeoenvironmental applications of the relationships between inorganic ash
957 chemistry and burn severity will likely be limited to being able to differentiate between more
958 and less severe burns.

959 PCA and Shapley value regression demonstrated that location and, to a lesser extent,
960 fire history also influence inorganic ash leachate chemistry. The PCA demonstrated that while
961 the first PC explained ash colour, the second PC explained location, with samples from
962 southeast Australia clustering differently to samples from southwest Australia. Shapley value
963 regression found that location was the dominant predictor of ash inorganic chemistry,
964 although for most elements, although ash colour was generally the second-most important
965 predictor. It should be noted that the collection of samples from southeast Australia was
966 delayed, and so the time the ashes spent degrading and reacting in the environment may be
967 more important than location, as suggested elsewhere (Sánchez-García et al.; 2023). Fire
968 histories, including the number of years since the last fire, and the total number of fires on
969 record for each collection point, had limited influence on ash leachate inorganic chemistry.
970 This is a positive outcome for palaeoenvironmental applications, as we can assume that there
971 is little memory in the system as fire history was generally a poor predictor of ash and soil
972 chemistry, and the chemistry of ash produced by each fire event should largely be
973 independent of past. This means that relative fire severities at a site should be able to be
974 determined after consideration of any vegetation or land use changes.

975 The relationship between ash leachate inorganic chemistry and elemental
976 volatilisation temperature did not wholly account for the differences in ash leachates by ash
977 colour. Competing factors which may explain why some analytes are higher in less
978 combusted ashes than in more combusted ashes (or vice versa) include that combustion
979 completeness may be independent of burn temperature, that pH affects the solubility of many
980 elements, that some metals will form complexes with organic matter, and that some ashes
981 potentially degraded prior to sampling (i.e. presumably removal of fine grains and dissolved
982 elements).

983 A comparison of ash leachate results presented here with those published elsewhere
984 showed significant heterogeneity in ash leachate inorganic geochemistry, including in how
985 geochemistry differed between black and white ashes. This suggests some level of site or
986 regional specificity, which is an important consideration for any palaeofire reconstruction. We
987 do note that our results showed good agreement with Miotliński et al. (2023), the only other
988 analysis of ash leachates from southwest Australia. For most elements, concentrations were
989 higher in ash leachates than in soil leachates. This is important for speleothem palaeofire
990 research, as it suggests the signal is sourced from ash, and not from soil, as seen elsewhere
991 (Hartland et al., 2012). Elements which are higher in soil leachates than in ash leachates (e.g.,
992 Fe) may be the key to finger-printing soil geochemical inputs. Key elements which should be
993 considered in future speleothem palaeofire include Na, K, Rb, Mn, P, As, Se, V, and Cl, and
994 SO₄, as these elements all varied significantly in leachates of black and white ashes, and are
995 all readily measured in calcite via LA-ICP-MS or SIMS (with sulphate measured as
996 elemental S), and are all generally of higher concentrations in ash leachates than in soil
997 leachates.

998 The preliminary biomarker results presented here were inconclusive, although PAH
999 concentrations were generally higher in black ash samples than in white ash samples, and
1000 levoglucosan concentrations were generally higher in grey and white samples than in black
1001 samples. While degradation *ex situ* may account for some inconsistency, further analyses are

1002 to establish the potential relationships between these biomarkers and burn severity, how these
1003 biomarkers degrade in nature, and the implications of for speleothem palaeofire research.

1004 **6 Acknowledgements**

1005 This research was funded by the Australian Research Council (DP200100203). MC
1006 was supported by an Early Career Research Grant from the Australian Institute of Nuclear
1007 Science and Engineering. We thank Yanchep National Parks staff, Calgardup Caves staff, the
1008 Kempsey Speleological Society, and Lachie MacCaw for assistance with sample collection.
1009 Thanks to Brett Rowling and Chris Vardanega at ANSTO ITNS for analyses of ash leachates.
1010 Thanks to Eve Slavich from UNSW Stats Central for statistical advice, and to Morgan
1011 Williams for productive conversation on the analysis of compositional data. Thanks also to
1012 Cameron Ritchie for helpful pointers on the geology of southwest WA, and to Tim Payne for
1013 discussion of leachate chemistry. We respectfully acknowledge the Whadjuk Noongar,
1014 Wadandi Noongar, and Dunghutti peoples as the traditional and spiritual custodians of the
1015 Yanchep (on Whadjuk Noongar boodja), Margaret River (on Wadandi boodja), and Macleay
1016 regions (on Dunghutti lands), where samples were collected for this research.

1017 **7 Open research**

1018 Data and scripts for the statistical analyses and data visualisation are available at
1019 <https://doi.org/10.6084/m9.figshare.25001858> (Campbell et al., 2024). These data are
1020 published under a CC BY 4.0 License. **Please note that for the original submission the**
1021 **editor has been supplied with a sharelink to the dataset.**

1022 **8 References**

- 1023 Adams, P.W., Boyle, J.R., 1980. Effects of Fire on Soil Nutrients in Clearcut and
1024 Whole-tree Harvest Sites in Central Michigan. *Soil Science Society of America Journal* 44,
1025 847–850. <https://doi.org/10.2136/sssaj1980.03615995004400040038x>
- 1026 American Public Health Association, American Water Works Association, Water
1027 Environment Federation, Baird, R.B., Eaton, A.D., Rice, E.W. (Eds.), 2017. *Standard*
1028 *Methods for the Examination of Water and Wastewater*, 23rd ed. APHA Press, Washington
1029 DC.
- 1030 Argiriadis, E., Denniston, R.F., Barbante, C., 2019. Improved Polycyclic Aromatic
1031 Hydrocarbon and n-Alkane Determination in Speleothems through Cleanroom Sample
1032 Processing. *Anal. Chem.* 91, 7007–7011. <https://doi.org/10.1021/acs.analchem.9b00767>
- 1033 Argiriadis, E., Denniston, R.F., Ondei, S., Bowman, D.M.J.S., Genuzio, G., Nguyen,
1034 H.Q.A., Thompson, J., Baltieri, M., Azenon, J., Cugley, J., Woods, D., Humphreys, W.F.,
1035 Barbante, C., 2023. Polycyclic aromatic hydrocarbons in tropical Australian stalagmites: a
1036 framework for reconstructing paleofire activity. *Geochimica et Cosmochimica Acta*.
1037 <https://doi.org/10.1016/j.gca.2023.11.033>
- 1038 Bai, J., Sun, X., Zhang, C., Xu, Y., Qi, C., 2013. The OH-initiated atmospheric
1039 reaction mechanism and kinetics for levoglucosan emitted in biomass burning. *Chemosphere*
1040 93, 2004–2010. <https://doi.org/10.1016/j.chemosphere.2013.07.021>
- 1041 Baker, A., Berthelin, R., Cuthbert, M.O., Treble, P.C., Hartmann, A., KSS Cave
1042 Studies Team, 2020. Rainfall recharge thresholds in a subtropical climate determined using a
1043 regional cave drip water monitoring network. *Journal of Hydrology* 587, 125001.
1044 <https://doi.org/10.1016/j.jhydrol.2020.125001>

- 1045 Balfour, V.N., Woods, S.W., 2013. The hydrological properties and the effects of
1046 hydration on vegetative ash from the Northern Rockies, USA. *CATENA* 111, 9–24.
1047 <https://doi.org/10.1016/j.catena.2013.06.014>
- 1048 Bento-Gonçalves, A., Vieira, A., Úbeda, X., Martin, D., 2012. Fire and soils: Key
1049 concepts and recent advances. *Geoderma*, Fire effects on soil properties 191, 3–13.
1050 <https://doi.org/10.1016/j.geoderma.2012.01.004>
- 1051 Beyene, M.T., Leibowitz, S.G., Dunn, C.J., Bladon, K.D., 2023. To burn or not to
1052 burn: An empirical assessment of the impacts of wildfires and prescribed fires on trace
1053 element concentrations in Western US streams. *Science of The Total Environment* 863,
1054 160731. <https://doi.org/10.1016/j.scitotenv.2022.160731>
- 1055 Bhattarai, H., Saikawa, E., Wan, X., Zhu, H., Ram, K., Gao, S., Kang, S., Zhang, Q.,
1056 Zhang, Y., Wu, G., Wang, X., Kawamura, K., Fu, P., Cong, Z., 2019. Levoglucosan as a tracer
1057 of biomass burning: Recent progress and perspectives. *Atmospheric Research* 220, 20–33.
1058 <https://doi.org/10.1016/j.atmosres.2019.01.004>
- 1059 Bivand, R., Keitt, T., Rowlingson, B., 2021. rgdal: Bindings for the “Geospatial” Data
1060 Abstraction Library.
- 1061 Blumenstock, M., Zimmermann, R., Schramm, K.-W., Kettrup, A., 2000. Influence of
1062 combustion conditions on the PCDD/F-, PCB-, PCBz- and PAH-concentrations in the post-
1063 combustion chamber of a waste incineration pilot plant. *Chemosphere* 40, 987–993.
1064 [https://doi.org/10.1016/S0045-6535\(99\)00343-4](https://doi.org/10.1016/S0045-6535(99)00343-4)
- 1065 Bodí, M.B., Martin, D.A., Balfour, V.N., Santín, C., Doerr, S.H., Pereira, P., Cerdà, A.,
1066 Mataix-Solera, J., 2014. Wildland fire ash: Production, composition and eco-hydro-
1067 geomorphic effects. *Earth-Science Reviews* 130, 103–127.
1068 <https://doi.org/10.1016/j.earscirev.2013.12.007>
- 1069 Bradstock, R.A., Auld, T.D., 1995. Soil Temperatures During Experimental Bushfires
1070 in Relation to Fire Intensity: Consequences for Legume Germination and Fire Management in
1071 South-Eastern Australia. *Journal of Applied Ecology* 32, 76–84.
1072 <https://doi.org/10.2307/2404417>
- 1073 Broadley, M., Brown, P., Cakmak, I., Rengel, Z., Zhao, F., 2012b. Function of
1074 Nutrients: Micronutrients, in: Marschner’s Mineral Nutrition of Higher Plants. Elsevier.
- 1075 Budescu, D.V., 1993. Dominance analysis: A new approach to the problem of relative
1076 importance of predictors in multiple regression. *Psychological Bulletin* 114, 542–551.
1077 <https://doi.org/10.1037/0033-2909.114.3.542>
- 1078 Burton, C.A., Hoefen, T.M., Plumlee, G.S., Baumberger, K.L., Backlin, A.R.,
1079 Gallegos, E., Fisher, R.N., 2016. Trace Elements in Stormflow, Ash, and Burned Soil
1080 following the 2009 Station Fire in Southern California. *PLOS ONE* 11, e0153372.
1081 <https://doi.org/10.1371/journal.pone.0153372>
- 1082 Campbell, G.S., Jungbauer, J.D.J., Bidlake, W.R., Hungerford, R.D., 1994. Predicting
1083 the effect of temperature on soil thermal conductivity. *Soil Science* 158, 307.
- 1084 Campbell, J.B., 1979. Spatial Variability of Soils. *Annals of the Association of*
1085 *American Geographers* 69, 544–556.
- 1086 Campbell, M., McDonough, L., Treble, P.C., Baker, A., Kosarac, N., Coleborn, K.,
1087 Wynn, P.M., Schmitt, A.K., 2023. A Review of Speleothems as Archives for Paleofire

1088 Proxies, With Australian Case Studies. *Reviews of Geophysics* 61, e2022RG000790.
1089 <https://doi.org/10.1029/2022RG000790>

1090 Campbell, M., Treble, P.C., McDonough, L.K., Naeher, S., Baker, A., Grierson, P.F.,
1091 Wong, H., Andersen, M.S., 2024. Australian Ash and Soil Leachate data and scripts.
1092 <https://doi.org/10.6084/m9.figshare.25001858>

1093 Campos, I., Vale, C., Abrantes, N., Keizer, J.J., Pereira, P., 2015. Effects of wildfire on
1094 mercury mobilisation in eucalypt and pine forests. *CATENA* 131, 149–159.
1095 <https://doi.org/10.1016/j.catena.2015.02.024>

1096 Canty, A., Ripley, B.D., 2022. *boot: Bootstrap R (S-Plus) Functions*.

1097 Carpenter, J., Bithell, J., 2000. Bootstrap confidence intervals: when, which, what? A
1098 practical guide for medical statisticians. *Statistics in Medicine* 19, 1141–1164.
1099 [https://doi.org/10.1002/\(SICI\)1097-0258\(20000515\)19:9<1141::AID-SIM479>3.0.CO;2-F](https://doi.org/10.1002/(SICI)1097-0258(20000515)19:9<1141::AID-SIM479>3.0.CO;2-F)

1100 Certini, G., 2005. Effects of fire on properties of forest soils: a review. *Oecologia* 143,
1101 1–10. <https://doi.org/10.1007/s00442-004-1788-8>

1102 Chapin, F.S., Matson, P.A., Vitousek, P.M., 2011. *Principles of Terrestrial Ecosystem*
1103 *Ecology*. Springer New York, New York, NY. <https://doi.org/10.1007/978-1-4419-9504-9>

1104 Chen, H., Chow, A.T., Li, X.-W., Ni, H.-G., Dahlgren, R.A., Zeng, H., Wang, J.-J.,
1105 2018. Wildfire Burn Intensity Affects the Quantity and Speciation of Polycyclic Aromatic
1106 Hydrocarbons in Soils. *ACS Earth Space Chem.* 2, 1262–1270.
1107 <https://doi.org/10.1021/acsearthspacechem.8b00101>

1108 Coleborn, K., Baker, Andy, Treble, P.C., Andersen, M.S., Baker, Andrew, Tadros,
1109 C.V., Tozer, M., Fairchild, I.J., Spate, A., Meehan, S., 2019. Corrigendum to “The impact of
1110 fire on the geochemistry of speleothem-forming drip water in a sub-alpine cave” [*Sci. Total*
1111 *Environ.* (2018) 408–420]. *Science of The Total Environment* 668, 1339–1340.
1112 <https://doi.org/10.1016/j.scitotenv.2019.02.350>

1113 Coleborn, K., Baker, Andy, Treble, P.C., Andersen, M.S., Baker, Andrew, Tadros,
1114 C.V., Tozer, M., Fairchild, I.J., Spate, A., Meehan, S., 2018. The impact of fire on the
1115 geochemistry of speleothem-forming drip water in a sub-alpine cave. *Science of The Total*
1116 *Environment* 642, 408–420. <https://doi.org/10.1016/j.scitotenv.2018.05.310>

1117 Croke, J., Vítkovský, J., Hughes, K., Campbell, M., Amirnezhad-Mozhdehi, S.,
1118 Parnell, A., Cahill, N., Dalla Pozza, R., 2021. A palaeoclimate proxy database for water
1119 security planning in Queensland Australia. *Sci Data* 8, 292. <https://doi.org/10.1038/s41597-021-01074-8>

1121 Costa, M.R., Calvão, A.R. and Aranha, J., 2014. Linking wildfire effects on soil and
1122 water chemistry of the Marão River watershed, Portugal, and biomass changes detected from
1123 Landsat imagery. *Applied Geochemistry* 44, 93-102.
1124 <https://doi.org/10.1016/j.apgeochem.2013.09.009>

1125 Dasgupta, S., Siegel, D.I., Zhu, C., Chanton, J.P., Glaser, P.H., 2015. Geochemical
1126 Mixing in Peatland Waters: The Role of Organic Acids. *Wetlands* 35, 567–575.
1127 <https://doi.org/10.1007/s13157-015-0646-2>

1128 Davison, A.C., Hinkley, D.V., 1997. *Bootstrap Methods and Their Applications*.
1129 Cambridge University Press, Cambridge.

1130 DeBano, L.F., 2000. The role of fire and soil heating on water repellency in wildland
1131 environments: a review. *Journal of Hydrology* 231–232, 195–206.
1132 [https://doi.org/10.1016/S0022-1694\(00\)00194-3](https://doi.org/10.1016/S0022-1694(00)00194-3)

1133 Denis, E.H., Toney, J.L., Tarozo, R., Scott Anderson, R., Roach, L.D., Huang, Y.,
1134 2012. Polycyclic aromatic hydrocarbons (PAHs) in lake sediments record historic fire events:
1135 Validation using HPLC-fluorescence detection. *Organic Geochemistry* 45, 7–17.
1136 <https://doi.org/10.1016/j.orggeochem.2012.01.005>

1137 Department of Environment and Conservation, 2010. Assessment levels for Soil,
1138 Sediment and Water, Contaminated Sites Management Series. Government of Western
1139 Australia.

1140 Dixon, D.J., Callow, J.N., Duncan, J.M.A., Setterfield, S.A., Pauli, N., 2022.
1141 Regional-scale fire severity mapping of Eucalyptus forests with the Landsat archive. *Remote*
1142 *Sensing of Environment* 270, 112863. <https://doi.org/10.1016/j.rse.2021.112863>

1143 Douglas, G., Hardenstine, J., Rouhani, S., Kong, D., Arnold, R., Gala, W., 2018.
1144 Chemical Preservation of Semi-volatile Polycyclic Aromatic Hydrocarbon Compounds at
1145 Ambient Temperature: A Sediment Sample Holding Time Study. *Arch Environ Contam*
1146 *Toxicol* 75, 486–494. <https://doi.org/10.1007/s00244-018-0517-y>

1147 Dunn, O.J., 1964. Multiple Comparisons Using Rank Sums. *Technometrics* 6, 241–
1148 252. <https://doi.org/10.2307/1266041>

1149 Elias, V.O., Simoneit, B.R.T., Cordeiro, R.C., Turcq, B., 2001. Evaluating
1150 levoglucosan as an indicator of biomass burning in Carajás, amazônia: a comparison to the
1151 charcoal record22Associate editor: R. Summons. *Geochimica et Cosmochimica Acta* 65,
1152 267–272. [https://doi.org/10.1016/S0016-7037\(00\)00522-6](https://doi.org/10.1016/S0016-7037(00)00522-6)

1153 Emmerton, C.A., Cooke, C.A., Hustins, S., Silins, U., Emelko, M.B., Lewis, T., Kruk,
1154 M.K., Taube, N., Zhu, D., Jackson, B., Stone, M., Kerr, J.G., Orwin, J.F., 2020. Severe
1155 western Canadian wildfire affects water quality even at large basin scales. *Water Research*
1156 183, 116071. <https://doi.org/10.1016/j.watres.2020.116071>

1157 Fontaine, J., 2022. Yanchep bushfire analysis – Black Summer final report. Nushfire
1158 and Natural Hazards CRC, Melbourne.

1159 Ford, D., Williams, P., 2007. *Karst Hydrogeology and Geomorphology*, 1st ed. Wiley.
1160 <https://doi.org/10.1002/9781118684986>

1161 Gabet, E.J., Bookter, A., 2011. Physical, chemical and hydrological properties of
1162 Ponderosa pine ash. *International Journal of Wildland Fire* 20, 443–452.
1163 <https://doi.org/10.1071/WF09105>

1164 Geoscience Australia. (2006). GEODATA TOPO 250K Series 3—(Personal
1165 Geodatabase format), Geoscience Australia, Canberra, dataset, viewed 18/01/2023. Retrieved
1166 from <http://pid.geoscience.gov.au/dataset/ga/63999>

1167 Giglio, L., van der Werf, G.R., Randerson, J.T., Collatz, G.J., Kasibhatla, P., 2006.
1168 Global estimation of burned area using MODIS active fire observations. *Atmospheric*
1169 *Chemistry and Physics* 6, 957–974. <https://doi.org/10.5194/acp-6-957-2006>

1170 Gillieson, D., Thurgate, M., 1999. Karst and agriculture in Australia. *International*
1171 *Journal of Speleology* 28. <https://dx.doi.org/10.5038/1827-806X.28.1.11>

1172 Granath, G., Evans, C.D. Strengbom, J., Fölster, J., Grelle, A., Strömqvist, J., Köhler,
1173 S.J., 2021. The impact of wildfire on biogeochemical fluxes and water quality in boreal
1174 catchments. *Biogeosciences* 18, 3243–3261. <https://doi.org/10.5194/bg-18-3243-2021>

1175 Granged, A.J.P., Zavala, L.M., Jordán, A., Bárcenas-Moreno, G., 2011. Post-fire
1176 evolution of soil properties and vegetation cover in a Mediterranean heathland after
1177 experimental burning: A 3-year study. *Geoderma* 164, 85–94.
1178 <https://doi.org/10.1016/j.geoderma.2011.05.017>

1179 Hageman, P.L., 2007. U.S. Geological Survey Field Leach Test for Assessing Water
1180 Reactivity and Leaching Potential of Mine Wastes, Soils, and Other Geologic and
1181 Environmental Materials (USGS Numbered Series No. 5-D3), U.S. Geological Survey Field
1182 Leach Test for Assessing Water Reactivity and Leaching Potential of Mine Wastes, Soils, and
1183 Other Geologic and Environmental Materials, Techniques and Methods.
1184 <https://doi.org/10.3133/tm5D3>

1185 Harris, J.A., 1915. On a Criterion of Substratum Homogeneity (Or Heterogeneity) in
1186 Field Experiments. *The American Naturalist* 49, 430–454. <https://doi.org/10.1086/279492>

1187 Hartland, A., Fairchild, I.J., Lead, J.R., Borsato, A., Baker, A., Frisia, S., Baalousha,
1188 M., 2012. From soil to cave: Transport of trace metals by natural organic matter in karst
1189 dripwaters. *Chemical Geology* 304–305, 68–82.
1190 <https://doi.org/10.1016/j.chemgeo.2012.01.032>

1191 Hartmann, A., Goldscheider, N., Wagener, T., Lange, J., Weiler, M., 2014. Karst water
1192 resources in a changing world: Review of hydrological modeling approaches. *Reviews of*
1193 *Geophysics* 52, 218–242. <https://doi.org/10.1002/2013RG000443>

1194 Hickenbottom, K., Pagilla, K., Hanigan, D., 2023. Wildfire impact on disinfection
1195 byproduct precursor loading in mountain streams and rivers. *Water Research* 244, 120474.
1196 <https://doi.org/10.1016/j.watres.2023.120474>

1197 Hogue, B.A., Inglett, P.W., 2012. Nutrient release from combustion residues of two
1198 contrasting herbaceous vegetation types. *Science of The Total Environment* 431, 9–19.
1199 <https://doi.org/10.1016/j.scitotenv.2012.04.074>

1200 Holland, E., 1994. The effects of fire on soluble rock landscapes. *Helictite* 32, 3–10.

1201 Hollander, M., Wolfe, D.A., 1973. *Nonparametric Statistical Methods*. John Wiley &
1202 Sons, New York.

1203 Homann, J., Karbach, N., Carolin, S.A., James, D.H., Hodell, D., Breitenbach, S.F.M.,
1204 Kwiecien, O., Brenner, M., Peraza Lope, C., Hoffmann, T., 2023. Past fire dynamics inferred
1205 from polycyclic aromatic hydrocarbons and monosaccharide anhydrides in a stalagmite from
1206 the archaeological site of Mayapan, Mexico. *Biogeosciences* 20, 3249–3260.
1207 <https://doi.org/10.5194/bg-20-3249-2023>

1208 Homann, J., Oster, J.L., de Wet, C.B., Breitenbach, S.F.M., Hoffmann, T., 2022.
1209 Linked fire activity and climate whiplash in California during the early Holocene. *Nat*
1210 *Commun* 13, 1–9. <https://doi.org/10.1038/s41467-022-34950-x>

1211 Humphreys, F.R., Lambert, M.J., 1965. An examination of a forest site which has
1212 exhibited the ash-bed effect. *Soil Res.* 3, 81–94. <https://doi.org/10.1071/sr9650081>

1213 Jiménez-Sánchez, M., Stoll, H., Vadillo, I., López-Chicano, M., Domínguez-Cuesta,
1214 M., Martín-Rosales, W., Meléndez-Asensio, M., 2008. Groundwater contamination in caves:

- 1215 four case studies in Spain. *International Journal of Speleology* 37.
1216 <http://dx.doi.org/10.5038/1827-806X.37.1.5>
- 1217 Johansson, I., van Bavel, B., 2003. Levels and patterns of polycyclic aromatic
1218 hydrocarbons in incineration ashes. *Science of The Total Environment* 311, 221–231.
1219 [https://doi.org/10.1016/S0048-9697\(03\)00168-2](https://doi.org/10.1016/S0048-9697(03)00168-2)
- 1220 Jones, M.W., Abatzoglou, J.T., Veraverbeke, S., Andela, N., Lasslop, G., Forkel, M.,
1221 Smith, A.J.P., Burton, C., Betts, R.A., van der Werf, G.R., Sitch, S., Canadell, J.G., Santín, C.,
1222 Kolden, C., Doerr, S.H., Le Quéré, C., 2022. Global and regional trends and drivers of fire
1223 under climate change. *Reviews of Geophysics* n/a, e2020RG000726.
1224 <https://doi.org/10.1029/2020RG000726>
- 1225 Karp, A.T., Holman, A.I., Hopper, P., Grice, K., Freeman, K.H., 2020. Fire
1226 distinguishers: Refined interpretations of polycyclic aromatic hydrocarbons for paleo-
1227 applications. *Geochimica et Cosmochimica Acta* 289, 93–113.
1228 <https://doi.org/10.1016/j.gca.2020.08.024>
- 1229 Key, C.H., Benson, N.C., 2006. Landscape Assessment (LA) (No. 164), IREMON:
1230 Fire effects monitoring and inventory system.
- 1231 Khanna, P.K., Raison, R.J., Falkiner, R.A., 1994. Chemical properties of ash derived
1232 from Eucalyptus litter and its effects on forest soils. *Forest Ecology and Management*,
1233 Ameliorative practices for restoring and maintaining 66, 107–125.
1234 [https://doi.org/10.1016/0378-1127\(94\)90151-1](https://doi.org/10.1016/0378-1127(94)90151-1)
- 1235 Kim, E.J., Choi, S.-D., Chang, Y.-S., 2011. Levels and patterns of polycyclic aromatic
1236 hydrocarbons (PAHs) in soils after forest fires in South Korea. *Environ Sci Pollut Res* 18,
1237 1508–1517. <https://doi.org/10.1007/s11356-011-0515-3>
- 1238 Kirkby, E., 2012. Introduction, Definition and Classification of Nutrients, in:
1239 Marschner's Mineral Nutrition of Higher Plants. Elsevier.
- 1240 Kuo, L.-J., Herbert, B.E., Louchouart, P., 2008. Can levoglucosan be used to
1241 characterize and quantify char/charcoal black carbon in environmental media? *Organic*
1242 *Geochemistry* 39, 1466–1478. <https://doi.org/10.1016/j.orggeochem.2008.04.026>
- 1243 Li, Y., Fu, T.-M., Yu, J.Z., Feng, X., Zhang, L., Chen, J., Boreddy, S.K.R., Kawamura,
1244 K., Fu, P., Yang, X., Zhu, L., Zeng, Z., 2021. Impacts of Chemical Degradation on the Global
1245 Budget of Atmospheric Levoglucosan and Its Use As a Biomass Burning Tracer. *Environ.*
1246 *Sci. Technol.* 55, 5525–5536. <https://doi.org/10.1021/acs.est.0c07313>
- 1247 Liang, J., 2021. ShapleyValue: Shapley Value Regression for Relative Importance of
1248 Attributes.
- 1249 Lipovetsky, S., Conklin, M., 2001. Analysis of regression in game theory approach.
1250 *Applied Stochastic Models in Business and Industry* 17, 319–330.
1251 <https://doi.org/10.1002/asmb.446>
- 1252 Lizundia-Loiola, J., Otón, G., Ramo, R., Chuvieco, E., 2020. A spatio-temporal
1253 active-fire clustering approach for global burned area mapping at 250 m from MODIS data.
1254 *Remote Sensing of Environment* 236, 111493. <https://doi.org/10.1016/j.rse.2019.111493>
- 1255 Marion, G.M., Moreno, J.M., Oechel, W.C., 1991. Fire Severity, Ash Deposition, and
1256 Clipping Effects on Soil Nutrients in Chaparral. *Soil Science Society of America Journal* 55,
1257 235–240. <https://doi.org/10.2136/sssaj1991.03615995005500010040x>

1258 Marlon, J.R., Bartlein, P.J., Carcaillet, C., Gavin, D.G., Harrison, S.P., Higuera, P.E.,
1259 Joos, F., Power, M.J., Prentice, I.C., 2008. Climate and human influences on global biomass
1260 burning over the past two millennia. *Nature Geosci* 1, 697–702.
1261 <https://doi.org/10.1038/ngeo313>

1262 McDonough, L.K., Treble, P.C., Baker, A., Borsato, A., Frisia, S., Nagra, G.,
1263 Coleborn, K., Gagan, M.K., Zhao, J., Paterson, D., 2022. Past fires and post-fire impacts
1264 reconstructed from a southwest Australian stalagmite. *Geochimica et Cosmochimica Acta*.
1265 <https://doi.org/10.1016/j.gca.2022.03.020>

1266 Meng, Q.-B., Wang, C.-K., Liu, J.-F., Zhang, M.-W., Lu, M.-M., Wu, Y., 2020.
1267 Physical and micro-structural characteristics of limestone after high temperature exposure.
1268 *Bull Eng Geol Environ* 79, 1259–1274. <https://doi.org/10.1007/s10064-019-01620-0>

1269 Millard, S.P., 2013. *EnvStats: An R Package for Environmental Statistics*. Springer,
1270 New York.

1271 Miotliński, K., Tshering, K., Boyce, M.C., Blake, D., Horwitz, P., 2023. Simulated
1272 temperatures of forest fires affect water solubility in soil and litter. *Ecological Indicators* 150,
1273 110236. <https://doi.org/10.1016/j.ecolind.2023.110236>

1274 Misra, M.K., Ragland, K.W., Baker, A.J., 1993. Wood ash composition as a function
1275 of furnace temperature. *Biomass and Bioenergy, Biomass in Combustion: The Challenge of*
1276 *Biomass?* 4, 103–116. [https://doi.org/10.1016/0961-9534\(93\)90032-Y](https://doi.org/10.1016/0961-9534(93)90032-Y)

1277 Muñoz-Rojas, M., Erickson, T.E., Martini, D., Dixon, K.W., Merritt, D.J., 2016. Soil
1278 physicochemical and microbiological indicators of short, medium and long term post-fire
1279 recovery in semi-arid ecosystems. *Ecological Indicators* 63, 14–22.
1280 <https://doi.org/10.1016/j.ecolind.2015.11.038>

1281 Nagra, G., Treble, P.C., Andersen, M.S., Fairchild, I.J., Coleborn, K., Baker, A., 2016.
1282 A post-wildfire response in cave dripwater chemistry. *Hydrol. Earth Syst. Sci.* 20, 2745–
1283 2758. <https://doi.org/10.5194/hess-20-2745-2016>

1284 NSW Department of Environment, Climate Change, and Water, 2011. *Guide to New*
1285 *South Wales Karst and Caves*.

1286 NSW Rural Fire Service, 2020. Spring fires torment northern NSW. *Bush Fire bulletin*
1287 42, 8–9.

1288 Otto, A., Gondokusumo, R., Simpson, M.J., 2006. Characterization and quantification
1289 of biomarkers from biomass burning at a recent wildfire site in Northern Alberta, Canada.
1290 *Applied Geochemistry* 21, 166–183. <https://doi.org/10.1016/j.apgeochem.2005.09.007>

1291 Panno, S.V., Kelly, W.R., Scott, J., Zheng, W., McNeish, R.E., Holm, N., Hoellein,
1292 T.J., Baranski, E.L., 2019. Microplastic Contamination in Karst Groundwater Systems.
1293 *Groundwater* 57, 189–196. <https://doi.org/10.1111/gwat.12862>

1294 Pebesma, E., 2018. Simple Features for R: Standardized Support for Spatial Vector
1295 Data. *The R Journal* 10, 439–446. <https://doi.org/10.32614/RJ-2018-009>

1296 Pebesma, E., Bivand, R., 2023. *Spatial Data Science: With Applications in R*, 1st ed.
1297 Chapman and Hall/CRC, Boca Raton. <https://doi.org/10.1201/9780429459016>

1298 Pellegrini, A.F.A., Harden, J., Georgiou, K., Hemes, K.S., Malhotra, A., Nolan, C.J.,
1299 Jackson, R.B., 2022. Fire effects on the persistence of soil organic matter and long-term
1300 carbon storage. *Nat. Geosci.* 15, 5–13. <https://doi.org/10.1038/s41561-021-00867-1>

1301 Pereira, P., Úbeda, X., 2010. Spatial distribution of heavy metals released from ashes
1302 after a wildfire. *Journal of Environmental Engineering and Landscape Management* 18, 13–
1303 22. <https://doi.org/10.3846/jeelm.2010.02>

1304 Pereira, P., Úbeda, X., Martin, D.A., 2012. Fire severity effects on ash chemical
1305 composition and water-extractable elements. *Geoderma, Fire effects on soil properties* 191,
1306 105–114. <https://doi.org/10.1016/j.geoderma.2012.02.005>

1307 Perrette, Y., Poulenard, J., Saber, A.-I., Fanget, B., Guittonneau, S., Ghaleb, B.,
1308 Garaudee, S., 2008. Polycyclic Aromatic Hydrocarbons in stalagmites: Occurrence and use
1309 for analyzing past environments. *Chemical Geology* 251, 67–76.
1310 <https://doi.org/10.1016/j.chemgeo.2008.02.013>

1311 Perrette, Y., Poulenard, J., Durand, A., Quiers, M., Malet, E., Fanget, B., Naffrechoux,
1312 E., 2013. Atmospheric sources and soil filtering of PAH content in karst seepage waters.
1313 *Organic Geochemistry* 65, 37–45. <https://doi.org/10.1016/j.orggeochem.2013.10.005>

1314 Playford, P.E., Cockbain, A.E., Low, G.H., 1976. *Geology of the Perth Basin Western*
1315 *Australia (Bulletin No. 124). Geological Survey of Western Australia.*

1316 Priestley, S.C., Treble, P.C., Griffiths, A.D., Baker, A., Abram, N.J., Meredith, K.T.,
1317 2023. Caves demonstrate decrease in rainfall recharge of southwest Australian groundwater is
1318 unprecedented for the last 800 years. *Commun Earth Environ* 4, 1–12.
1319 <https://doi.org/10.1038/s43247-023-00858-7>

1320 Puth, M.-T., Neuhäuser, M., Ruxton, G.D., 2015. On the variety of methods for
1321 calculating confidence intervals by bootstrapping. *Journal of Animal Ecology* 84, 892–897.
1322 <https://doi.org/10.1111/1365-2656.12382>

1323 QGIS Development Team, 2022. QGIS Geographic Information System, version 3.28.
1324 QGIS Association.

1325 Qian, Y., Miao, S.L., Gu, B., Li, Y.C., 2009. Effects of Burn Temperature on Ash
1326 Nutrient Forms and Availability from Cattail (*Typha domingensis*) and Sawgrass (*Cladium*
1327 *jamaicense*) in the Florida Everglades. *Journal of Environmental Quality* 38, 451–464.
1328 <https://doi.org/10.2134/jeq2008.0126>

1329 Quintana, J.R., Cala, V., Moreno, A.M., Parra, J.G., 2007. Effect of heating on mineral
1330 components of the soil organic horizon from a Spanish juniper (*Juniperus thurifera* L.)
1331 woodland. *Journal of Arid Environments* 71, 45–56.
1332 <https://doi.org/10.1016/j.jaridenv.2007.03.002>

1333 R Core Team, 2023. R: A Language and Environment for Statistical Computing. R
1334 Foundation for Statistical Computing, Vienna, Austria.

1335 Reberski, J., Terzić, J., Maurice, L.D., Lapworth, D.J., 2022. Emerging organic
1336 contaminants in karst groundwater: A global level assessment. *Journal of Hydrology* 604,
1337 127242. <https://doi.org/10.1016/j.jhydrol.2021.127242>

1338 Rehn, E., Rowe, C., Ulm, S., Woodward, C., Bird, M., 2021. A late-Holocene
1339 multiproxy fire record from a tropical savanna, eastern Arnhem Land, Northern Territory,
1340 Australia. *The Holocene* 31, 870–883. <https://doi.org/10.1177/0959683620988030>

1341 Rey-Salgueiro, L., Martínez-Carballo, E., Merino, A., Vega, J.A., Fonturbel, M.T.,
1342 Simal-Gandara, J., 2018. Polycyclic Aromatic Hydrocarbons in Soil Organic Horizons
1343 Depending on the Soil Burn Severity and Type of Ecosystem. *Land Degradation &*
1344 *Development* 29, 2112–2123. <https://doi.org/10.1002/ldr.2806>

- 1345 Roshan, A., Biswas, A., 2023. Fire-induced geochemical changes in soil: Implication
1346 for the element cycling. *Science of The Total Environment* 868, 161714.
1347 <https://doi.org/10.1016/j.scitotenv.2023.161714>
- 1348 Rosner, B., 1983. Percentage Points for a Generalized ESD Many-Outlier Procedure.
1349 *Technometrics* 25, 165–172. <https://doi.org/10.1080/00401706.1983.10487848>
- 1350 Rost, H., Loibner, A.P., Hasinger, M., Braun, R., Szolar, O.H.J., 2002. Behavior of
1351 PAHs during cold storage of historically contaminated soil samples. *Chemosphere* 49, 1239–
1352 1246. [https://doi.org/10.1016/S0045-6535\(02\)00497-6](https://doi.org/10.1016/S0045-6535(02)00497-6)
- 1353 Roy, D.P., Boschetti, L., Maier, S.W., Smith, A.M.S., 2010. Field estimation of ash
1354 and char colour-lightness using a standard grey scale. *Int. J. Wildland Fire* 19, 698.
1355 <https://doi.org/10.1071/WF09133>
- 1356 Rubino, M., D’Onofrio, A., Seki, O., Bendle, J.A., 2016. Ice-core records of biomass
1357 burning. *The Anthropocene Review* 3, 140–162. <https://doi.org/10.1177/2053019615605117>
- 1358 Sánchez-García, C., Santín, C., Neris, J., Sigmund, G., Otero, X.L., Manley, J.,
1359 González-Rodríguez, G., Belcher, C.M., Cerdà, A., Marcotte, A.L., Murphy, S.F., Rhoades,
1360 C.C., Sheridan, G., Strydom, T., Robichaud, P.R., Doerr, S.H., 2023. Chemical characteristics
1361 of wildfire ash across the globe and their environmental and socio-economic implications.
1362 *Environment International* 178, 108065. <https://doi.org/10.1016/j.envint.2023.108065>
- 1363 Santín, C., Doerr, S.H., Otero, X.L., Chafer, C.J., 2015. Quantity, composition and
1364 water contamination potential of ash produced under different wildfire severities.
1365 *Environmental Research* 142, 297–308. <https://doi.org/10.1016/j.envres.2015.06.041>
- 1366 Santín, C., Doerr, S.H., Shakesby, R.A., Bryant, R., Sheridan, G.J., Lane, P.N.J.,
1367 Smith, H.G., Bell, T.L., 2012. Carbon loads, forms and sequestration potential within ash
1368 deposits produced by wildfire: new insights from the 2009 ‘Black Saturday’ fires, Australia.
1369 *Eur J Forest Res* 131, 1245–1253. <https://doi.org/10.1007/s10342-012-0595-8>
- 1370 Sasowsky, I.D. (Ed.), 2000. Groundwater flow and contaminant transport in carbonate
1371 aquifers. Balkema, Rotterdam.
- 1372 Serrasolsas, I., Khanna, P.K., 1995. Changes in heated and autoclaved forest soils of
1373 S.E. Australia. II. Phosphorus and phosphatase activity. *Biogeochemistry* 29, 25–41.
1374 <https://doi.org/10.1007/BF00002592>
- 1375 Shafizadeh, F., Furneaux, R.H., Cochran, T.G., Scholl, J.P., Sakai, Y., 1979.
1376 Production of levoglucosan and glucose from pyrolysis of cellulosic materials. *Journal of*
1377 *Applied Polymer Science* 23, 3525–3539. <https://doi.org/10.1002/app.1979.070231209>
- 1378 Shakesby, R.A., Doerr, S.H., 2006. Wildfire as a hydrological and geomorphological
1379 agent. *Earth-Science Reviews* 74, 269–307. <https://doi.org/10.1016/j.earscirev.2005.10.006>
- 1380 Shi, K., Touge, Y., 2022. Characterization of global wildfire burned area
1381 spatiotemporal patterns and underlying climatic causes. *Sci Rep* 12, 644.
1382 <https://doi.org/10.1038/s41598-021-04726-2>
- 1383 Simon, E., Choi, S.-D., Park, M.-K., 2016. Understanding the fate of polycyclic
1384 aromatic hydrocarbons at a forest fire site using a conceptual model based on field
1385 monitoring. *Journal of Hazardous Materials* 317, 632–639.
1386 <https://doi.org/10.1016/j.jhazmat.2016.06.030>
- 1387 Simoneit, B.R.T., Schauer, J.J., Nolte, C.G., Oros, D.R., Elias, V.O., Fraser, M.P.,
1388 Rogge, W.F., Cass, G.R., 1999. Levoglucosan, a tracer for cellulose in biomass burning and

1389 atmospheric particles. *Atmospheric Environment* 33, 173–182.
1390 [https://doi.org/10.1016/S1352-2310\(98\)00145-9](https://doi.org/10.1016/S1352-2310(98)00145-9)

1391 Stronach, N.R.H., McNaughton, S.J., 1989. Grassland Fire Dynamics in the Serengeti
1392 Ecosystem, and a Potential Method of Retrospectively Estimating Fire Energy. *Journal of*
1393 *Applied Ecology* 26, 1025–1033. <https://doi.org/10.2307/2403709>

1394 Suci, L.G., Masiello, C.A., Griffin, R.J., 2019. Anhydrosugars as tracers in the Earth
1395 system. *Biogeochemistry* 146, 209–256. <https://doi.org/10.1007/s10533-019-00622-0>

1396 Treble, P.C., Fairchild, I.J., Baker, A., Meredith, K.T., Andersen, M.S., Salmon, S.U.,
1397 Bradley, C., Wynn, P.M., Hankin, S.I., Wood, A., McGuire, E., 2016. Roles of forest
1398 bioproductivity, transpiration and fire in a nine-year record of cave dripwater chemistry from
1399 southwest Australia. *Geochimica et Cosmochimica Acta* 184, 132–150.
1400 <https://doi.org/10.1016/j.gca.2016.04.017>

1401 Úbeda, X., Pereira, P., Outeiro, L., Martin, D.A., 2009. Effects of fire temperature on
1402 the physical and chemical characteristics of the ash from two plots of cork oak (*Quercus*
1403 *suber*). *Land Degradation & Development* 20, 589–608. <https://doi.org/10.1002/ldr.930>

1404 Ulery, A.L., Graham, R.C., Amrhein, C., 1993. Wood-ash composition and soil pH
1405 following intense burning. *Soil Science* 156, 358–364.

1406 Vachula, R.S., Huang, Y., Longo, W.M., Dee, S.G., Daniels, W.C., Russell, J.M.,
1407 2019. Evidence of Ice Age humans in eastern Beringia suggests early migration to North
1408 America. *Quaternary Science Reviews* 205, 35–44.
1409 <https://doi.org/10.1016/j.quascirev.2018.12.003>

1410 Vesper, D.J., Loop, C.M., White, W.B., 2003. Contaminant transport in karst aquifers.
1411 *Speleogenesis and Evolution of Karst Aquifers* 1, 2–11.

1412 Vilhar, U., Kermavnar, J., Kozamernik, E., Petrič, M., Ravbar, N., 2022. The effects
1413 of large-scale forest disturbances on hydrology – An overview with special emphasis on karst
1414 aquifer systems. *Earth-Science Reviews* 235, 104243.
1415 <https://doi.org/10.1016/j.earscirev.2022.104243>

1416 Vu, V.Q., 2011. ggbiplot: A ggplot2 based biplot.

1417 Wakeham, S.G., Schaffner, C., Giger, W., 1980. Polycyclic aromatic hydrocarbons in
1418 Recent lake sediments—I. Compounds having anthropogenic origins. *Geochimica et*
1419 *Cosmochimica Acta* 44, 403–413. [https://doi.org/10.1016/0016-7037\(80\)90040-X](https://doi.org/10.1016/0016-7037(80)90040-X)

1420 Wei, M., Zhang, Z., Long, T., He, G., Wang, G., 2021. Monitoring Landsat Based
1421 Burned Area as an Indicator of Sustainable Development Goals. *Earth's Future* 9.
1422 <https://doi.org/10.1029/2020EF001960>

1423 Wickham, H., 2022. stringr: Simple, Consistent Wrappers for Common String
1424 Operations.

1425 Wickham, H., 2016. ggplot2: Elegant Graphics for Data Analysis.

1426 Wickham, H., Francois, R., Henry, L., Muller, K., 2020. dplyr: A Grammar of Data
1427 Manipulation.

1428 Wickham, H., Henry, L., 2023. purrr: Functional Programming Tools.

1429 Wickham, H., Hester, J., Bryan, J., 2023. readr: Read Rectangular Text Data.

1430 Williams, P.R., Congdon, R.A., Grice, A.C., Clarke, P.J., 2004. Soil temperature and
1431 depth of legume germination during early and late dry season fires in a tropical eucalypt

- 1432 savanna of north-eastern Australia. *Austral Ecology* 29, 258–263.
1433 <https://doi.org/10.1111/j.1442-9993.2004.01343.x>
- 1434 Wu, G., Wang, D.Y., 2012. Mechanical and Acoustic Emission Characteristics of
1435 Limestone after High Temperature. *Advanced Materials Research* 446–449, 23–28.
1436 <https://doi.org/10.4028/www.scientific.net/AMR.446-449.23>
- 1437 Yang, Y., Zhang, N., Xue, M., Tao, S., 2010. Impact of soil organic matter on the
1438 distribution of polycyclic aromatic hydrocarbons (PAHs) in soils. *Environmental Pollution*,
1439 *Advances of air pollution science: from forest decline to multiple-stress effects on forest*
1440 *ecosystem services* 158, 2170–2174. <https://doi.org/10.1016/j.envpol.2010.02.019>
- 1441 Yusiharni, E., Gilkes, R., 2012. Minerals in the ash of Australian native plants.
1442 *Geoderma* 189–190, 369–380. <https://doi.org/10.1016/j.geoderma.2012.06.035>
- 1443 Zennaro, P., Kehrwald, N., Marlon, J., Ruddiman, W.F., Brücher, T., Agostinelli, C.,
1444 Dahl-Jensen, D., Zangrando, R., Gambaro, A., Barbante, C., 2015. Europe on fire three
1445 thousand years ago: Arson or climate? *Geophysical Research Letters* 42, 5023–2033.
1446 <https://doi.org/10.1002/2015GL064259>
- 1447 Zomer, R.J., Xu, J., Trabucco, A., 2022. Version 3 of the Global Aridity Index and
1448 Potential Evapotranspiration Database. *Sci Data* 9, 409. [https://doi.org/10.1038/s41597-022-](https://doi.org/10.1038/s41597-022-01493-1)
1449 [01493-1](https://doi.org/10.1038/s41597-022-01493-1)
- 1450 **9 References from the Supporting Information**
- 1451 Alshehri, T., Wang, J., Singerling, S.A., Gigault, J., Webster, J.P., Matiassek, S.J.,
1452 Alpers, C.N., Baalousha, M., 2023. Wildland-urban interface fire ashes as a major source of
1453 incidental nanomaterials. *Journal of Hazardous Materials* 443, 130311.
1454 <https://doi.org/10.1016/j.jhazmat.2022.130311>
- 1455 Balfour, V.N., Woods, S.W., 2013. The hydrological properties and the effects of
1456 hydration on vegetative ash from the Northern Rockies, USA. *CATENA* 111, 9–24.
1457 <https://doi.org/10.1016/j.catena.2013.06.014>
- 1458 Burton, C.A., Hoefen, T.M., Plumlee, G.S., Baumberger, K.L., Backlin, A.R.,
1459 Gallegos, E., Fisher, R.N., 2016. Trace Elements in Stormflow, Ash, and Burned Soil
1460 following the 2009 Station Fire in Southern California. *PLOS ONE* 11, e0153372.
1461 <https://doi.org/10.1371/journal.pone.0153372>
- 1462 Douglas, G., Hardenstine, J., Rouhani, S., Kong, D., Arnold, R., Gala, W., 2018.
1463 Chemical Preservation of Semi-volatile Polycyclic Aromatic Hydrocarbon Compounds at
1464 Ambient Temperature: A Sediment Sample Holding Time Study. *Arch Environ Contam*
1465 *Toxicol* 75, 486–494. <https://doi.org/10.1007/s00244-018-0517-y>
- 1466 Johansen, M.P., Hakonson, T.E., Whicker, F.W., Breshears, D.D., 2003. Pulsed
1467 Redistribution of a Contaminant Following Forest Fire: Cesium-137 in Runoff. *Journal of*
1468 *Environmental Quality* 32, 2150–2157.
- 1469 Ku, P., Tsui, M.T.-K., Nie, X., Chen, H., Hoang, T.C., Blum, J.D., Dahlgren, R.A.,
1470 Chow, A.T., 2018. Origin, Reactivity, and Bioavailability of Mercury in Wildfire Ash.
1471 *Environ. Sci. Technol.* 52, 14149–14157. <https://doi.org/10.1021/acs.est.8b03729>
- 1472 Miotliński, K., Tshering, K., Boyce, M.C., Blake, D., Horwitz, P., 2023. Simulated
1473 temperatures of forest fires affect water solubility in soil and litter. *Ecological Indicators* 150,
1474 110236. <https://doi.org/10.1016/j.ecolind.2023.110236>

1475 Pebesma, E., 2018. Simple Features for R: Standardized Support for Spatial Vector
1476 Data. *The R Journal* 10, 439–446. <https://doi.org/10.32614/RJ-2018-009>

1477 Pebesma, E., Bivand, R., 2023. *Spatial Data Science: With Applications in R*, 1st ed.
1478 Chapman and Hall/CRC, Boca Raton. <https://doi.org/10.1201/9780429459016>

1479 Pereira, P., Úbeda, X., Martín, D.A., 2012. Fire severity effects on ash chemical
1480 composition and water-extractable elements. *Geoderma, Fire effects on soil properties* 191,
1481 105–114. <https://doi.org/10.1016/j.geoderma.2012.02.005>

1482 Quintana, J.R., Cala, V., Moreno, A.M., Parra, J.G., 2007. Effect of heating on mineral
1483 components of the soil organic horizon from a Spanish juniper (*Juniperus thurifera* L.)
1484 woodland. *Journal of Arid Environments* 71, 45–56.
1485 <https://doi.org/10.1016/j.jaridenv.2007.03.002>

1486 Sánchez-García, C., Santín, C., Neris, J., Sigmund, G., Otero, X.L., Manley, J.,
1487 González-Rodríguez, G., Belcher, C.M., Cerdà, A., Marcotte, A.L., Murphy, S.F., Rhoades,
1488 C.C., Sheridan, G., Strydom, T., Robichaud, P.R., Doerr, S.H., 2023. Chemical characteristics
1489 of wildfire ash across the globe and their environmental and socio-economic implications.
1490 *Environment International* 178, 108065. <https://doi.org/10.1016/j.envint.2023.108065>

1491 Úbeda, X., Pereira, P., Outeiro, L., Martín, D.A., 2009. Effects of fire temperature on
1492 the physical and chemical characteristics of the ash from two plots of cork oak (*Quercus*
1493 *suber*). *Land Degradation & Development* 20, 589–608. <https://doi.org/10.1002/ldr.930>

1494 Wickham, H., 2016. *ggplot2: Elegant Graphics for Data Analysis*.

1495 Wickham, H., Francois, R., Henry, L., Muller, K., 2020. *dplyr: A Grammar of Data*
1496 *Manipulation*.

1497

1498

1499

1500

1501